Title

Transcriptome and DNA methylome divergence of inflorescence development between 2 ecotypes in Panicum hallii

Journal

Plant Physiology, 192(3)

ISSN

0032-0889

Authors

Weng, Xiaoyu
Song, Haili
Sreedasyam, Avinash
et al.

Publication Date

2023-07-03

DOI

10.1093/plphys/kiad209

Peer reviewed

Short title: Genomic divergence of *Panicum hallii* inflorescence

Transcriptome and DNA methylome divergence of inflorescence development between two ecotypes in *Panicum hallii*

Xiaoyu Weng (翁小煜)[a*], Haili Song[a], Avinash Sreedasyam[b], Taslima Haque[a], Li Zhang[a], Cindy Chen[c], Yuko Yoshinaga[c], Melissa Williams[b], Ronan C. O'Malley[c], Jane Grimwood[b], Jeremy Schmutz[b], and Thomas E. Juenger[a*]

[a]Department of Integrative Biology, University of Texas at Austin, Austin, TX, USA

[b]HudsonAlpha Institute for Biotechnology, Huntsville, AL, USA

[c]US Department of Energy Joint Genome Institute, Lawrence Berkeley National Laboratory, Berkeley, CA, USA

***Address correspondence to:**

Xiaoyu Weng, University of Texas at Austin, Department of Integrative Biology

xiaoyu.weng@utexas.edu (X.Y.W.)

Thomas E. Juenger, University of Texas at Austin, Department of Integrative Biology

tjuenger@austin.utexas.edu (T.E.J.)

One-sentence summary:

A comparative transcriptome and DNA methylome analysis of different stages of inflorescence between upland and lowland ecotypes reveals gene expression and DNA methylation divergence in *Panicum hallii*.

Author Contributions

X.Y.W. and T.E.J. designed the experiments. X.Y.W., C.C., Y.Y., M.W., R.O.M., J.G., and J.S. carried out the experiments and collected the data. X.Y.W., S.H.L., A.S., T.H., L.Z., and T.E.J. analyzed the data. X.Y.W. and T.E.J. wrote the manuscript with input from all other authors. All authors read and approved the final manuscript.

The authors responsible for distribution of materials integral to the findings presented in this article in accordance with the policy described in the Instructions for Authors (https://academic.oup.com/plphys/pages/General-Instructions) are Thomas E. Juenger and Xiaoyu Weng.

Abstract

The morphological diversity of the inflorescence determines flower and seed production, which is critical for plant adaptation. Hall's panicgrass (*Panicum hallii*, *P. hallii*) is a wild perennial grass that has been developed as a model to study perennial grass biology and adaptive evolution. Highly divergent inflorescences have evolved between the two major ecotypes in *P. hallii*, the upland ecotype (*P. hallii var hallii*, HAL2 genotype) with compact inflorescence and large seed and the lowland ecotype (*P. hallii var filipes*, FIL2 genotype) with an open inflorescence and small seed. Here we conducted a comparative analysis of the transcriptome and DNA methylome, an epigenetic mark that influences gene expression regulation, across different stages of inflorescence development using genomic references for each ecotype. Global transcriptome analysis of differentially expressed genes (DEGs) and co-expression modules underlying the inflorescence divergence revealed the potential role of cytokinin signaling in

heterochronic changes. Comparing DNA methylome profiles revealed a remarkable level of differential DNA methylation associated with the evolution of *P. hallii* inflorescence. We found that a large proportion of differentially methylated regions (DMRs) were located in the flanking regulatory regions of genes. Intriguingly, we observed a substantial bias of CHH hypermethylation in the promoters of FIL2 genes. The integration of DEGs, DMRs, and K_a/K_s ratio results characterized the evolutionary features of DMRs-associated DEGs that contribute to the divergence of the *P. hallii* inflorescence. This study provides insights into the transcriptome and epigenetic landscape of inflorescence divergence in *P. hallii* and a genomic resource for perennial grass biology.

Introduction

Flowering plants have evolved diverse inflorescence architecture, which has a direct effect on the spatial arrangement of inflorescence branching and the production of flowers and seeds (Harder and Prusinkiewicz, 2013; Kellogg, 2022). The extensive diversity of inflorescence architecture is shaped by a combination of genetic, epigenetic, and environmental factors, with critical economic importance in agricultural crops and profound ecological implications in wild species (Barazesh and McSteen, 2008; Teo et al., 2014; Tu et al., 2019). Recently, progress has been made in understanding the area of natural genetic architecture underlying inflorescence development, largely focusing on the model plants Arabidopsis (*Arabidopsis thaliana*) and several important crops, including rice (*Oryza sativa*), maize (*Zea mays*), common wheat (*Triticum aestivum*), and Setaria (*Setaria viridis*) (Kellogg et al., 2013; Zhang and Yuan, 2014).

This accumulated knowledge provides an opportunity to better understand the role of inflorescence diversity in the adaptive evolution of wild plants.

DNA methylation is a heritable epigenetic modification that contributes to gene regulation and genome structure and integrity (Chan et al., 2005; Law and Jacobsen, 2010; Zhang et al., 2018). In land plants, DNA methylation occurs at the cytosine bases with three sequence contexts (CG, CHG and CHH, where H represents A, T or C). Genome-scale DNA methylation analyses show extensive variation among different plant species in all three DNA methylation contexts, with the predominant form being CG methylation compared with CHG and CHH methylation (Niederhuth et al., 2016). The classic model assumes that the addition of DNA methylation in the promoters of genes typically represses gene expression by recruiting repressor proteins (Tate and Bird, 1993). Recently, a growing body of research has revealed that gene body methylation can be positively associated with gene expression and may shape important features of plant genome evolution (Bewick and Schmitz, 2017). DNA methylation plays an essential role in a wide range of growth and development events, especially in the developmental complexity of inflorescence architecture (Zhang et al., 2018; Tu et al., 2019). This perspective is supported by evidence that most loss-of-function mutations of genes involved in DNA methylation establishment and maintenance show abnormal inflorescence morphology (Moritoh et al., 2012; Fernandez-Nohales et al., 2014; Liao et al., 2019). Additionally, epigenetic alleles involving DNA methylation variation have been identified in the key regulators of inflorescence development (Zhu et al., 2013; Zhang et al., 2017; Xu et al., 2020). These findings suggest that DNA methylation may be of crucial importance in the evolution of the structure and organization of the inflorescence.

High-throughput sequencing techniques have been used extensively for genome-wide profiling of gene expression and DNA methylation to study a variety of developmental processes (Yang et al., 2015; Huang et al., 2019; Rajkumar et al., 2020; Shi et al., 2021). As the key determinant of productivity, the inflorescence of many crop species has been studied with detailed developmental stage-specific transcriptome profiling (Furutani et al., 2006; Wang et al., 2010; Eveland et al., 2014; Harrop et al., 2016; Feng et al., 2017; Zhu et al., 2018). For example, stage- and meristem-specific gene expression profiles have provided a genome-wide view of regulatory networks controlling young panicle development in rice (Furutani et al., 2006; Wang et al., 2010; Harrop et al., 2016) and wheat (Feng et al., 2017). Moreover, whole-genome analysis of DNA methylation has found epigenetic mechanisms that coordinate gene structure and expression during inflorescence development (Li et al., 2012; Parvathaneni et al., 2020; Sun et al., 2020). For instance, single-base resolution methylome studies have assessed the functional importance of epigenetic differentiation of young panicle between wild and cultivated rice (Li et al., 2012). Genome-wide DNA methylation profiling integrated with other multi-omics analysis has revealed the role of chromatin interactions that coordinate *trans* and *cis* regulation of differential expression between two separate types of inflorescence (ear and tassel) in maize (Sun et al., 2020). These advances provide not only a deep understanding of the relationship between complex gene regulatory networks and epigenetic modifications but also help to identify the potential candidates controlling inflorescence morphology and grain yield.

Hall's panicgrass (*Panicum hallii*, *P. hallii*) is a native perennial C_4 grass with a distribution in southwestern regions of North America (Lowry et al., 2015). Due to a close evolutionary

relationship to the polyploid biofuel crop switchgrass (*Panicum virgatum*), *P. hallii* has been developed as a complementary diploid model system (Lovell et al., 2018). *P. hallii* is found in a wide range of soil and ecological conditions, spanning from xeric inland regions to mesic coastal areas (Gould et al., 2018; Palacio-Mejia et al., 2021). *P. hallii* populations have diverged into two major ecotypes (or varieties), *P. hallii var. hallii* (hereafter *var. hallii*) and *P. hallii var. filipes* (hereafter *var. filipes*) (Lowry et al., 2015; Lovell et al., 2018). Similar to other upland plants, the widespread *var. hallii* is typically found in drier habitats with shallow and rocky soils (Palacio-Mejia et al., 2021). In contrast, the more geographically restricted *var. filipes* commonly grows in Gulf coast areas in clay soils and mesic depressions (Palacio-Mejia et al., 2021). Whole genome sequencing and assemblies suggest that *var hallii* and *var filipes* shared a common ancestor ~1.08 million years ago (Lovell et al., 2018). Although there is some evidence of hybridization between these ecotypes, it is rare in nature and they exhibit considerable population structure and genomic and phenotypic divergence, including notable differences in flowering time, plant size and inflorescence architecture (Palacio-Mejia et al., 2021). In general, *var. hallii* flowers earlier than *var. filipes* and is distinguished from the latter by its sparse inflorescence and larger seed. Recently, genetic resources derived from the crossing of *var. hallii* with *var. filipes* have been developed for studying the genetic basis of ecotype-differentiating traits (e.g., flowering time, flower number, seed mass, etc.), shoot-root resource acquisition traits, and seed dormancy and seedling characteristics (Lowry et al., 2015; Khasanova et al., 2019; Razzaque and Juenger, 2022). Transcriptome studies have been undertaken with the goal of understanding how *P. hallii* responds to various environmental cues (Lovell et al., 2016; Weng et al., 2019). Nevertheless, gene expression divergence associated with the evolution of ecotype-specific morphology and its relationship with the global patterns of DNA methylation variation remain poorly understood in

P. hallii.

In this study, we performed a comparative transcriptome and DNA methylome analysis at different stages of inflorescence development contrasting the two ecotypes of *P. hallii* using RNA sequencing and whole-genome bisulfite sequencing. Global analysis of transcriptome data identified the heterochronic patterns of DEGs between the two types of *P. hallii* inflorescences over development. Similarly, comparing whole-genome DNA methylation profiles allowed a characterization of DNA methylation divergence during the evolution and development of *P. hallii* inflorescence. An integrated analysis of DMRs, DEGs, and K_a/K_s ratio highlighted the evolutionary features of candidate genes that might determine the phenotypic diversity of inflorescence branching architecture and seed size in *P. hallii*. Together, this study provides insights into transcriptome and epigenetic landscape of inflorescence divergence in *P. hallii*.

Results

Distinct phenotypes of inflorescence and seed between two *P. hallii* ecotypes

To provide tools for studying *P. hallii* evolutionary genomics, we have developed reference genomes spanning the wide ecotypic divergence observed in *P. hallii* (Lovell et al., 2018). Our genome assemblies have been derived from two accessions, *P. hallii var. hallii* (HAL2) and *P. hallii var. filipes* (FIL2), that are representative of the upland and lowland ecotypes in *P. hallii* (Lovell et al., 2018). In this study, we investigate inflorescence development and divergence between HAL2 and FIL2. As shown in Figure 1A, *P. hallii* has a panicle-type inflorescence with many branches supporting spikelet development and seed set. The inflorescence of HAL2 exhibits a remarkably different branching patterns compared with that in FIL2, mainly in the

reduction of both primary and secondary branch numbers (Figure 1, A and C), and its compact rather than open structure. This divergent architecture results in a significant decrease in spikelet numbers in HAL2 (Figure 1C). In contrast, we observed significantly enlarged seed size in HAL2 relative to FIL2, as measured by hundred-seed-weight (Figure 1, B and C). These observations suggested that divergence in inflorescence architecture in *P. hallii* may be associated with a trade-off between seed size and number in *P. hallii* as has been observed in many domesticated grasses (Sadras, 2007). To determine the developmental origin of the differences, we performed scanning electron microscope (SEM) experiments to compare the inflorescence between HAL2 and FIL2 at the early stages (D1 and D2, see method for details). We observed a strong gradient of development at the D1 stage, which included both later branching meristems and floral meristems (Supplemental Figure S1). While the D2 stage is mainly spikelet meristems and floral meristems, it still has branching meristems at the base (Supplemental Figure S1). SEM imagery showed that the number of branching meristems was substantially higher in FIL2 compared to HAL2 (Supplemental Figure S1), which likely explains the morphological difference in inflorescence between HAL2 and FIL2.

Genome-wide analysis of gene expression divergence between two *P. hallii* inflorescences

To explore this divergent inflorescence development, RNA-seq experiments were performed on four stages of inflorescence tissues, designated as D1-D4 of HAL2 and FIL2 (2 genotypes × 4 developmental stages × 3 biological replicates = 24 libraries) (Figure 2A, see method for details). After filtering genes with low expression, 19,332 one-to-one orthologous genes were detected in the dataset for downstream analysis. There were strong correlations among the biological replicates ($r > 0.97$), supporting the high quality and reproducibility of the entire dataset.

Principal component analysis of expressed genes revealed a strong global structure along the development gradient and related to genotype divergence (Figure 2B). The first component explained 57% of the expression variance and clearly distinguished the stages across the developmental gradient, while the second component explained 35% of the expression variance and mainly discriminated between samples from HAL2 and FIL2 (Figure 2B). The first two components explained the vast majority of variance (92%), suggesting the dominance of development and genotype effects in the entire dataset.

To analyze the molecular basis of expression divergence, we applied linear models on gene counts to test the effects of genotype, development, and genotype × development interaction on gene expression across the entire transcriptome (see method for details). We identified 12,633 genes (65.3%) with significant genotype effects ($q_{geno} < 0.01$) and 15,602 genes (80.7%) with significant expression level changes across the developmental gradient ($q_{devo} < 0.01$) (Figure 2C and Supplemental Table S1). Meanwhile, we detected 5,078 genes (26.3%) with significant interaction between development and genotype ($q_{int} < 0.01$) (Figure 2C and Supplemental Table S1), with the magnitude or direction of gene expression divergence between HAL2 and FIL2 depended on the specific stage of development. We only detected 1,907 genes (9.9%) with strictly additive genotype effects, which are genes with consistent difference between HAL2 and FIL2 regardless of developmental stages (Figure 2C and Supplemental Table S1). Similarly, we detected 3,966 genes (20.5%) exhibiting strictly additive developmental effects without genotype influences (genotype and/or interaction effects) (Figure 2C and Supplemental Table S1). Finally, we found that 7,285 genes (37.7%) were detected with independent genotype and development effects, but without significant interaction effects (Figure 2C and Supplemental Table S1). After

examining genes exhibiting significant genotype and/or interaction effects (q-value < 0.01), we concluded that 14,270 genes (73.8%) showed expression divergence between HAL2 and FIL2 inflorescence (Figure 2C and Supplemental Table S1).

Heterochronic changes in gene expression divergence during inflorescence development

Our SEM results revealed heterochrony of inflorescence development, a divergence in the timing of development between the two ecotypes. Thus, we primarily focused on 5,078 interaction genes that could be responsible for this phenomenon. We conducted a stage-by-stage contrast of genes with diverged expression between HAL2 and FIL2 inflorescence to determine the direction of differential expression (q-value < 0.01, Supplemental Table S2). We found that the vast majority of interaction genes (4,533, 89.3%) showed patterns with consistently greater expression in one of the ecotypes (Figure 3A); for convenience, we call these HAL2 or FIL2 predominant expression patterns. We did not observe a directional bias in the pattern of predominant genes, since 2,274 genes showed HAL2 predominant patterns and 2,259 genes exhibited FIL2 predominant patterns (Figure 3A). As example, we identified putative orthologs controlling flowering time (*CONSTANS-LIKE 4* (*COL4*), *MADS-BOX TRANSCRIPTION FACTOR 51* (*MADS51*), *PSEUDO-RESPONSE REGULATOR 37* and *73* (*PRR37* and *PRR73*)), organ development (*ORYZA SATIVA HOMEOBOX 15* (*OSH15*), *GRAIN SIZE 5* (*GS5*), *SUPERNUMERARY BRACT* (*SNB*)), hormone pathways (*CYTOKININ DEHYDROGENASE 1* and *5* (*CKX1* and *CKX5*), *PIN-FORMED 1* (*PIN1*), *GIBBERELLIN 2-OXIDASE 7* (*GA2ox7*)), and small RNA biogenesis (*DICER-LIKE PROTEIN 2A* (*DCL2a*)) among these genes (Figure 3B). These candidates could be either HAL2 or FIL2 predominant expression patterns (Figure 3B), which have pleiotropic effects in inflorescence development in many grass systems (Bouche

et al., 2006; Lee et al., 2007; Barazesh and McSteen, 2008; Yan et al., 2013). We found 493 genes (9.7%) with rank changing patterns of relative repression or induction changes between genotypes at different development stages (Figure 3A). These genes had either an opposite direction or a remarkable magnitude difference in gene expression divergence. Many of them were associated with multiple stress pathways, including putative orthologs of *IMPAIRED IN BABA-INDUCED STERILITY 1* (*IBS1*), *ORGANELLE RNA RECOGNITION MOTIF-CONTAINING 3* (*ORRM3*), *SULFITE REDUCTASE* (*SIR*), *PYRROLINE-5-CARBOXYLATE SYNTHETASE 2* (*P5CS2*), *WRKY DNA-BINDING PROTEIN 21* (*WRKY21*), and *CBL-INTERACTING PROTEIN KINASE 20* (*CIPK20*) (Figure 3B).

To further gain insight into the divergence patterns across developmental gradients, we conducted a clustering analysis for the 5,078 interaction genes. The minimum centroid distance was used to determine the number of cluster cores (*c*) (Supplemental Figure S2). This analysis led to the detection of 5 core clusters representing the divergence pattern of interaction gene expression across development, ranging from 681 to 1,528 genes in each cluster (Figure 4A and Supplemental Table S3). The expression of genes in clusters 1 and 2 had an increasing tendency across developmental gradients (Figure 4A). By contrast, genes in cluster 3 had expression that gradually decreased with the maturation of the inflorescence (Figure 4A). The majority of genes in clusters 4 and 5 displayed FIL2 and HAL2 predominant patterns, respectively (Figure 4A). We next performed Gene Ontology (GO) enrichment analysis for each cluster, in which the significance was determined by the False Discovery Rate (FDR) corrected p-value < 0.05. This analysis identified GO terms that were significantly enriched in each cluster, e.g., photosynthesis and response to cytokinin terms in cluster 1; ion transmembrane transport and multiple response

to stresses terms in cluster 2; chromosome organization, DNA replication, cell cycle, gene expression, and mRNA processing terms in cluster 3; regulation of ethylene-activated signaling pathway and intracellular signal transduction terms in cluster 4; and photorespiration term in cluster 5 (top terms in Figure 4B, the full list in Supplemental Table S4). We were particularly interested in the expression patterns of genes in an enriched GO term of "response to cytokinin" (GO:0009735) (FDR corrected *p*-value = 0.0086) in cluster 1, as cytokinin is often a key factor in determining the architecture of the inflorescence. The genes in this enriched term were putative orthologs of *GATA TRANSCRIPTION FACTOR 21* (*GATA21*), *HISTIDINE-CONTAINING PHOSPHOTRANSFER 2* (*HP2*), ribosomal protein (*RIBOSOMAL PROTEIN UL5C* (*RPL5*), *RIBOSOMAL PROTEIN UL13C* (*RPL13*), *RIBOSOMAL PROTEIN BL27C* (*RPL27*), and *RIBOSOMAL PROTEIN S1* (*RPS1*), and other genes involved in the modulation of cytokinin homeostasis (Figure 4C). Intriguingly, the increasing trend across developmental gradients of these genes in HAL2 is much stronger than that in FIL2 (Figure 4C), suggesting that heterochronic changes in the timing of cytokinin signaling could be a crucial driver in the divergence of HAL2 and FIL2 inflorescence development.

We also note that there is a large number of genes (7,285) with independent genotype and development effects. The directions and distribution of differentially expressed genes (DEGs) in this group are depicted in Supplemental Figure S3. After conducting a clustering analysis of this gene set, we identified 6 core clusters with different patterns of gene expression behavior (Supplemental Figure S2 and Supplemental Figure S4A). Among them, genes in clusters 1 and 2 had an increasing tendency across developmental gradients, while genes in clusters 3 and 4 decreased the expression with the maturation of the inflorescence (Supplemental Figure S4A).

The majority of genes in clusters 5 and 6 displayed FIL2 and HAL2 predominant patterns, respectively (Supplemental Figure S4A). We identified an enriched GO term of "response of auxin" (GO:0009733) in cluster 1, which included putative orthologs of *INDOLE-3-ACETIC ACID INDUCIBLE 4* and *31* (*IAA4* and *IAA31*) and *MYB DOMAIN PROTEIN 12*, *94*, and *96* (*MYB12*, *MYB94*, and *MYB96*) (Supplemental Figure S4, B and C; Supplemental Table S4). We observed a considerable number of significantly enriched GO terms in clusters 3 and 4, many of which had a shared function in metabolic processes, gene expression, and DNA repair (Supplemental Figure S4B and Supplemental Table S4). Intriguingly, we detected enriched GO terms of "maintenance of inflorescence meristem identity" (GO:0010077) and "flower development" (GO:0009908) in cluster 4, which included the putative orthologs of *BEL1-LIKE HOMEODOMAIN 8* and *9* (*BLH8* and *BLH9*) and *MADS-BOX TRANSCRIPTION FACTOR 15*, *17*, and *58* (*MADS15*, *MADS17*, *MADS58*) (Supplemental Figure S4, B and C; Supplemental Table S4). Moreover, we found an enriched GO term of "methylation" (GO:0032259) in cluster 4, which included the putative orthologs involved in epigenetic silencing and *de novo* methylation (*PROTEIN ARGININE METHYLTRANSFERASE 5* (*PRMT5*), *RNA-DIRECTED DNA METHYLATION 12* (*RDM12*), *METHYLTRANSFERASE 1* (*MET1*), and *EMBRYONIC FLOWER 2* (*EMF2*)) (Supplemental Figure S4, B and C; Supplemental Table S4). Although not identified as interaction genes, these genes may still contribute to the expression divergence between HAL2 and FIL2 inflorescence. Finally, we found enriched GO terms of photosynthesis in cluster 2, macromolecule modification in cluster 5, and plastid organization in cluster 6 (Supplemental Figure S4B and Supplemental Table S4).

For 1,907 genes with strictly additive genotype effects, we identified 2 core clusters with

different predominant patterns (Supplemental Figure S2 and Supplemental Figure S5A). Enriched GO terms were not identified in these clusters, however, we observed the putative orthologs involved in flowering time (*EARLY HEADING DATE 3* (*Ehd3*)) and GA signaling (*GIBBERELLIC ACID INSENSITIVE* (*GAI*)) pathways with HAL2 predominant patterns (cluster 1) and putative orthologs involved in DNA methylation (*METHYL-CPG-BINDING DOMAIN 10* (*MBD10*)) and early flower development (*MADS-BOX TRANSCRIPTION FACTOR 3* (*MADS3*)) pathways with FIL2 predominant patterns (cluster 2) (Supplemental Figure S5B). For 3,966 genes with strictly additive development effects, we identified 4 core clusters that were considered co-expressed (Supplemental Figure S2 and Supplemental Figure S6A). We identified a large number of GO terms that were significantly enriched in cluster 1, including the terms of metabolic processes, chromosome organization, gene expression, RNA splicing, cell cycle, and DNA recombination (Supplemental Figure S6B and Supplemental Table S4). We observed a decreasing tendency of putative orthologs of *LONELY GUY* (*LOG*) and *RICE FLORICULA/LEAFY* (*RFL*) in cluster 1 (Supplemental Figure S6C), which are associated with meristem activity and initiation (Kurakawa et al., 2007; Rao et al., 2008). Finally, we identified enriched GO terms of vesicle transport in cluster 2 and cell wall biogenesis in cluster 3 (Supplemental Figure S6B and Supplemental Table S4). As development progressed, the expression of genes in these terms (e.g., GO:0009834, plant-type secondary cell wall biogenesis) increased gradually, with no expression difference between the two ecotypes (Supplemental Figure S6C).

Global methylome profiles of different *P. hallii* inflorescences

As methylation-related genes and enriched GO terms were identified in the divergence

expression analysis, we generated single-base resolution maps of DNA methylation using bisulfite sequencing to explore the possible function of DNA methylation in *P. hallii* inflorescence divergence. We utilized the same paired inflorescence tissues from HAL2 and FIL2 at the early (D1) and late (D4) stages from our RNA-seq studies for DNA methylation analysis (2 genotypes × 2 developmental stages × 3 biological replicates = 12 libraries). After removal of adapter contaminates and low-quality reads, a total of ~1.9 billion paired-end reads were generated across our samples. We observed a strong mapping bias by performing alignments of the same sequencing reads from all inflorescence samples to both the HAL2 and FIL2 reference genomes. Mapping efficiencies dramatically dropped from ~75% when aligned to "self" genomes to ~30% when aligned to incorrect genomes (Supplemental Figure S7 and Supplemental Table S5), demonstrating substantial sequence divergence between HAL2 and FIL2, especially in non-coding regions. Therefore, we mapped reads from each genotype to their respective genomes for further analysis. We found that approximately 73% of CG sites, 68% of CHG sites, and 55% of CHH sites were covered by at least five uniquely mapped reads across different genotypes and tissues (Supplemental Figure S8). We observed high bisulfite conversion rates, with an average level of 97.5% using a chloroplast control (Supplemental Table S5), that there was little strand differentiation, and the three biological replicates of each sample were highly correlated with each other ($r > 0.95$). These results suggested that our data were reproducible and sufficient for further analysis.

Genome-wide DNA methylation level analyses revealed that a large proportion of CG (~66%) and CHG (~49%) sites have methylated cytosines, while the level of CHH methylation (~3.1%) was comparatively low (Figure 5B). The genome-wide degree of CG methylation was

stable across genotypes and developmental stages, however, we observed a significant difference in non-CG methylation levels (especially in CHH methylation) between genotypes or development stages (p-value < 0.05) (Figure 5B). Global methylation levels revealed that around 32% of CG and 40% of CHG sites had low methylation levels (< 0.2), and about 64% of CG and 32% of CHG sites showed high methylation levels (> 0.8), while CHH site levels were overall very low, with about 97% in the low methylation level category (< 0.2) and less than 0.2% had high methylation levels (> 0.8) (Supplemental Figure S9). The distributions of methylation levels were further compared in three contexts across chromosomes (Figure 5A and Supplemental Figure S10). We observed a broad hyper CG and CHG methylation region for each chromosome, which is highly negatively correlated with gene density (r = -0.974 to -0.976 for CG in all samples; r = -0.975 to -0.976 for CHG in all samples) (Figure 5A and Supplemental Figure S10). These regions are clearly associated with pericentromeres, which have been identified in recent *P. hallii* genomic studies (Lovell et al., 2018). We found a strong positive correlation between CHH methylation levels and gene density in most samples (r = 0.573 in HAL2-D1, r = 0.741 in FIL2-D1, r = 0.626 in FIL2-D4) (Figure 5A). Intriguingly, this positive correlation was relatively weak in HAL2 inflorescence at the late stage (r = 0.199 in HAL2-D4) (Supplemental Figure S10).

To understand the relationship between DNA methylation and gene expression, we profiled DNA methylation levels across gene bodies for genes with different expression levels. Genes were divided into six groups based on expression, from a silent rank1 (count = 0) to the highest rank6 (Supplemental Figure S11). We observed that genes with low expression, especially the genes with no expression in rank1, have higher CG and CHG methylation level at the promoter

and the 3' end regulatory regions (Figure 5C and Supplemental Figure S12). Notably, we found that genes with high expression, especially the genes in rank6 and rank5, have higher CG methylation level at the gene body regions (Figure 5C and Supplemental Figure S12). These patterns were observed across both genotypes and all development stages (Figure 5C and Supplemental Figure S12), suggesting the methylation levels in promoter regions were generally associated with transcriptional silencing while the methylation levels of gene-body regions were more often positively associated with gene expression levels.

Differential DNA methylation between different *P. hallii* inflorescences

To determine differentially methylated regions, we compared methylation levels across different genomic regions in one-to-one putative orthologs between two genotypes (HAL2 vs FIL2) or two development stages (D1 vs D4). A gene with a significantly different proportion of methylation in any of the three methylation contexts across at least one annotated feature was considered a differentially methylated gene (DMGs) (q-value < 0.01, methylation level change > 0.1, see method for details). A total of 10,509 DMGs were detected between HAL2 and FIL2 across development stages; 8,414 of them were from the earliest stage, and 8,073 of them were from the late stage (Figure 6; Supplemental Figure S13; and Supplemental Table S6). We found 5,589 (23.8%) DMGs in the CG context, 3,055 (13.0%) DMGs in the CHG context, and 3,817 (16.2%) DMGs in the CHH context at the early stage (Figure 6 and Supplemental Table S6). Similarly, a total of 5,035 (21.4%) DMGs in the CG context, 2,962 (12.6%) DMGs in the CHG context, and 4,066 DMGs in the CHH context were detected at the late stage (Supplemental Figure S13 and Supplemental Table S6). In addition, we detected 4,047 differentially methylated intergenic regions (2,878 in the CG context, 2,849 in the CHG context, and 1,042 in the CHH

393 context) at the early stage and 3,790 differentially methylated intergenic regions (2,628 in the
394 CG context, 2,726 in the CHG context, and 847 in the CHH context) at the late stage
395 (Supplemental Figure S14 and Supplemental Table S7). Notably, our analysis revealed that the
396 flanking regions of genes (e.g., promoter, 5'UTR, and 3'UTR) are more frequently differentially
397 methylated than the regions within genes (e.g., exons and introns) (Figure 6 and Supplemental
398 Figure S13). Intriguingly, we found a genome-wide bias of CHH hypermethylation in the
399 promoter region in FIL2 (Figure 6; Supplemental Figure S13; and Supplemental Figure S15),
400 suggesting the potential role of CHH methylation in inflorescence divergence in *P. hallii*.
401 Further, we compared the methylation levels between early and late stages of inflorescences in
402 each genotype. We only detected 1,189 (5.1%) DMGs associated with HAL2 inflorescence
403 development and 1,017 (4.3%) DMGs associated with FIL2 inflorescence development
404 (Supplemental Figure S16 and Supplemental Table S8), suggesting that methylation levels are
405 relatively stable during inflorescence development in *P. hallii*.
406
407 **The patterns of DMRs-associated DEGs evolution during inflorescence divergence**
408 To understand the role of DNA methylation in driving the expression of genes involved in the
409 inflorescence diversity, we identified DMRs-associated DEGs between the ecotypes by joining
410 the results of our methylome and transcriptome datasets. DMRs-associated DEGs analysis was
411 conducted on a set of 7,843 genes with divergent expression that were differentially expressed
412 under stringent criteria (q-value < 0.01, fold change > 1.5) in the stage-by-stage contrasts
413 analysis (Supplemental Table S2). In this criteria, a total of 1,745 and 2,180 genes at D1 and D4
414 stages, respectively, were identified as DMRs-associated DEGs between HAL2 and FIL2
415 inflorescences (Supplemental Figure S17), suggesting that more than one third of DEGs were

associated with the methylation changes (42.2% in D1 and 38.6% in D4). Among them, 1,279 genes in CG context, 714 genes in CHG context, and 802 genes in CHH context were detected as DMRs-associated DEGs at D1 stage (Supplemental Figure S17). Similarly, 1,488 genes in CG context, 827 genes in CHG context, and 1,083 genes in CHH context were detected as DMRs-associated DEGs at D4 stage (Supplemental Figure S17). Overall, DMRs-associated DEGs with CG context differential methylation were more abundant than other sequence contexts. We observed that a larger fraction of DMRs-associated DEGs had differences in methylation at the flanking regulatory regions, especially the promoter and 3'UTR regions (Figure 7 and Supplemental Figure S18). We noticed that CHH hypermethylation in the FIL2 promoter regions could be associated with either gene activation or repression (Figure 7 and Supplemental Figure S18). Intriguingly, we did not observe a simple pattern between the direction of differential methylation and differential gene expression at both stages of inflorescence development (Figure 7 and Supplemental Figure S18). The trend between direction of differential methylation and differential gene expression could be positive or negative in all three sequence contexts located in the five different genic regions (Figure 7 and Supplemental Figure S18). Similar findings are reported in recent studies (Rajkumar et al., 2020; Li et al., 2021), suggesting the complex role DNA methylation plays in gene expression regulation.

To explore protein evolution associated with DMRs-associated DEGs, we compared the K_a/K_s ratio (non-synonymous substitutions per non-synonymous sites/synonymous substitutions per synonymous sites) for HAL2 and FIL2 gene pairs between DMRs-associated DEGs and the genome-wide pattern for one-to-one putative orthologs. The K_a/K_s ratio of DMRs-associated DEGs and one-to-one putative orthologs centered around a peak at 0.55 and 0.46 (Figure 8A),

respectively. No statistically significant difference of the K_a/K_s ratio distribution was observed between DMRs-associated DEGs and the genome-wide backgrounds. We observed that only 302 (~12.6%) of DMRs-associated DEGs pairs have K_a/K_s ratios > 1 (Figure 8B and Supplemental Table S9), suggesting that the majority of DMRs-associated DEGs are evolving under purifying selection. Among the DMRs-associated DEGs under positive selection, we identified candidates involved in hormone pathways, including the putative orthologs of *GIBBERELLIN 2-OXIDASE 3* (*GA2ox3*) and *RESPONSE REGULATOR 12* (*RR12*) (Figure 8C). These genes have been shown to play a role in gibberellin catabolism and cytokinin signaling, respectively (Bolduc and hake, 2009; Dai et al., 2017). Moreover, we detected the putative ortholog of *NUCLEAR FACTOR Y, SUBUNIT C10* (*NF-YC10*), which is associated with flowering time, inflorescence regulation, and seed size in rice (Figure 8C) (Jia et al., 2019; Zhang et al., 2019). Among these genes, the putative ortholog of *GA2ox3* was differentially expressed with strictly additive genotype effects, while the putative orthologs of *RR12* and *NF-YC10* were differentially expressed with independent genotype and development effects (Figure 8D). Differential methylation and expression of these positively selective genes may play an important role in the evolution of *P. hallii* inflorescences.

Discussion

The inflorescence branching system of a plant species influences the number of flowers and seeds the plant produces. This, in turn, affects the reproductive success of plants through their life history strategies, as well as the economic potential of the crops. Genome-wide gene expression and DNA methylation analyses are now widely used to study the genetic and epigenetic mechanisms of inflorescence development from a variety of important crops (Furutani

et al., 2006; Wang et al., 2010; Li et al., 2012; Eveland et al., 2014; Feng et al., 2017; Parvathaneni et al., 2020; Sun et al., 2020). Despite ever-increasing knowledge of grass inflorescence development (Kellogg, 2022), an effective model of inflorescence patterning from wild species without a domestication history is still lacking. *P. hallii* is a native perennial C_4 grass with a highly diverse and complex inflorescence with striking divergence between ecotypes adapted to contrasting habitats (Lowry et al., 2015; Palacio-Mejia et al., 2021). To date, *P. hallii* has been developed as a complementary diploid model in parallel with domesticated crops and other C_4 perennial grasses (Lovell et al., 2018). A systematic comparison of inflorescence transcriptome and DNA methylome for *P. hallii* ecotypes should provide insights into the molecular mechanisms leading to their divergent inflorescences.

Divergence and heterochronic expression of inflorescence development in *P. hallii*

Previous transcriptomic studies have revealed the regulatory modules of young inflorescence development in major crops including rice, maize, and wheat (Furutani et al., 2006; Wang et al., 2010; Eveland et al., 2014; Harrop et al., 2016; Feng et al., 2017). These studies provide resources to identify potential targets for genetic engineering and overall crop improvement. However, most of these studies performed experiments within a single genetic background, and therefore provide limited information about the evolution of gene regulatory networks associated with traits under selection. Using *P. hallii* as a model wild perennial grass, we designed a two-factor factorial experiment to understand gene expression divergence and development. Despite only ~1.08 Mya of divergence (Lovell et al., 2018), we demonstrated that the vast majority of genes (14,270, 73.8%) exhibited significant expression divergence between HAL2 and FIL2 inflorescence or significant expression level changes across development. Among them, we

detected a considerable number of genes (5,078, 26.3%) that exhibit a significant interaction between development and genotype, suggesting the potential role of heterochronic expression during the development of inflorescence evolution in *P. hallii*. Heterochronic change is an alteration in the timing of developmental programs during evolution, which are known to contribute to the evolution of inflorescence architecture (Buendia-Monreal and Gillmor, 2018). In grasses, the inflorescence branching systems are determined by the timing of phase transition from the branch meristem to the spikelet meristem (Kyozuka et al., 2014). Delays in the spikelet meristem specification result in more complex and larger inflorescences (Kyozuka et al., 2014). In our study, we observed heterochronic shifts for interaction genes potentially controlling flowering time, organ development, and hormone pathways. For example, *PRR37* is a key component in the core circadian feedback loop controlling flowering time, inflorescence architecture, and adaptation (Koo et al., 2013; Yan et al., 2013). Our findings suggested that the putative ortholog of *PRR37* had a greater expression in FIL2 than HAL2 at an earlier developmental stage (Figure 3B). The *AP2* family gene, *SNB*, has been identified as a heterochronic gene controlling the transition from spikelet meristem to floral meristem and the floral organ development (Lee et al., 2007; Wang et al., 2015). Our data show that the putative ortholog of *SNB* had a greater expression in FIL2 than HAL2 at a later developmental stage (Figure 3B). The *cytokinin oxidases*, *CKXs*, have been observed to regulate cytokinin accumulation in inflorescence meristems and the number of reproductive organs (Ashikari et al., 2005; Bartrina et al., 2011). Our results identified two putative orthologs of *CKXs* (*CKX1* and *CKX5*) with opposite predominant patterns and heterochronic changes (Figure 3B). Moreover, we identified a significantly enriched GO term of "response to cytokinin" (GO:0009735) in cluster 1 of interaction genes. We observed that the majority of these cytokinin response genes

have potential heterochronic expression changes, that is a greater expression in HAL2 than FIL2 at a later developmental stage. The heterochronic expression of genes involving in cytokinin signaling and catabolism pathways may play a role in the divergence of the inflorescence development between the *P. hallii* ecotypes. It was noticed that a large number of genes (7,285) have been identified to have independent genotype and development effects. We found a significantly enriched GO term of "response to auxin" (GO:0009733) in cluster 1 of this category gene. It is well established that auxin signaling plays a role in the formation of axillary meristems and inflorescences development (Deveshwar et al., 2020). Further, we observed several putative orthologs of *MADS* transcription factors in an enriched GO terms of "flower development" (GO:0009908) in cluster 4 of this category gene. These *MADS* genes expressed higher in FIL2 relative to HAL2, with a general pattern of decreasing expression with development. It was known that *MADS* genes control inflorescence branching systems via the regulation of meristem identification and development in grasses (Liu et al., 2013; Kyozuka et al., 2014). Despite not being identified as interaction effects, these genes were still thought to be playing a role in the expression divergence between HAL2 and FIL2 inflorescence.

DNA methylation and the evolution of inflorescence development in *P. hallii*

In this study, we performed whole-genome bisulfite sequencing to understand the role of DNA methylation during inflorescence development and architecture divergence. In our methylome study in *P. hallii*, we found that the overall methylation levels from tissues across different genotypes and development stages were similar in each context. The proportions of methylated cytosines in CG, CHG, and CHH contexts were 66%, 49%, and 3.1%, respectively. For comparison, values reported in *Arabidopsis* are 30.5% for CG, 10.0% for CHG, and 3.9% for

CHH, in rice are 58.4% of CG, 31.0% of CHG, and 5.1% for CHH, and in maize are 86% of CG, 74% of CHG, and 5.4% for CHH (Niederhuth et al., 2016). These results suggested that *P. hallii* has an intermediate level of DNA methylation. Coincident with previous findings, we observed a strong positive association between CG and CHG methylation with gene density, suggesting the role of DNA methylation in the establishment and maintenance of centromeric and pericentromeric heterochromatin regions. We also found a positive association between CHH methylation and gene density (except in HAL2-D4 samples). Previous studies have shown that methylation at CHH sites is kept high in rice reproductive organs compared to vegetative tissues (Higo et al., 2020). Our analysis of the relationship between gene expression and DNA methylation level suggested that non-expressed and lowly-expressed genes showed higher CG and CHG methylation levels in their proximal regulatory regions, while genes expressed at high levels were highly CG methylated within their gene body regions. These patterns are similar to recent results reported in chickpea and pineapple (Rajkumar et al., 2020; Shi et al., 2021), suggesting the conserved antagonistic role of CG methylation in gene expression regulation in the regulatory and gene body regions.

Previous studies have shown that mapping bias to a single genome can introduce clear and substantial quantification bias in the identification of DMRs (Wulfridge et al., 2019). Notably, most methylome studies align to a single reference genome to identify DMRs between different genotypes due to the limitation of genomic resources (Li et al., 2012; Rajkumar et al., 2020). Our previous studies have developed reference genomes for HAL2 and FIL2 and investigated the genome size divergence between the two ecotypes (487 Mb in HAL vs 535 Mb in FIL2) (Lovell et al., 2018). Here, we observed a dramatic drop in mapping efficiencies from alignments to

554 individual genomes (HAL2 to HAL2 and FIL2 to FIL2, ~75%) compared to alignments to
555 divergent genomes (HAL2 to FIL2 and FIL2 to HAL2, ~30%). After mapping reads to their own
556 individual genome references, we found that almost half of one-to-one putative orthologs
557 (10,509) are differentially methylated in at least one feature of genomic regions between HAL2
558 and FIL2 across inflorescence development. This degree of widespread natural variation in DNA
559 methylation was also observed in a diverse panel of Arabidopsis and maize (Kawakatsu et al.,
560 2016; Xu et al., 2020). Interestingly, previous studies showed that differential methylation
561 primarily occurs within gene body regions (Rajkumar et al., 2020). However, we observed that
562 flanking regulatory regions, including promoter, 5'UTR, and 3'UTR, are more frequently
563 differentially methylated than the regions within gene body regions. One explanation for this
564 conflicting pattern could be difference in alignment strategy, as most of these studies mapped
565 reads from different genotypes to one genome reference and probably induced quantification bias
566 in the highly variable regulatory regions. Intriguingly, we observed a significant bias of CHH
567 hypermethylation in the promoters of FIL2 genes. Unlike CG and CHG methylation, CHH
568 methylation is more dynamic and is deposited *de novo* every generation (Martin et al., 2021).
569 This genome-wide pattern of CHH hypermethylation in the promoter regions of FIL2 genes
570 might be associated with population expansion in *P. hallii* from the coast to inland and may
571 contribute to local adaptation through gene expression regulation related to morphological and
572 physiological change. Although tissue or developmental stage specific methylation patterns have
573 been mentioned in some studies (Huang et al., 2019), we only detected a few DMGs between
574 two stages of development. Considering that a large number of one-to-one putative orthologs are
575 differentially expressed across development stages, other processes beyond differential
576 methylation are likely to be involved in the observed expression variation.

Finally, we detected 2,911 DMRs-associated DEGs between HAL2 and FIL2 across inflorescence development. The relationship between the direction of differential methylation in different sequence contexts and differential gene expression is not simple, including both positively and negatively associated patterns. This complex pattern was also observed in recent studies in other species (Rajkumar et al., 2020; Li et al., 2021). Although recent evidence from population level studies suggested that selection on DNA methylation could be weak, differential methylation of key development genes are associated with phenotypic variation (Xu et al., 2020). In our study, we identified the putative orthologs of *GA2ox3* and *RR12* as DMRs-associated DEGs. The gibberellin catabolism gene is a direct target of *KNOTTED1* (*KN1*), a key transcription factor involved in the establishment and maintenance of plant meristems (Bolduc and hake, 2009). It was reported that *RR12* functions as a molecular link between cytokinin signaling and the expression of shoot meristem genes *WUSCHEL* (*WUS*) (Dai et al., 2017). Interestingly, both of the hormone genes are potentially under positive selection. Functional validation of DMRs-associated DEGs in future studies will provide insights into the evolutionary processes driving the divergence of inflorescence morphology in *P. hallii*.

Materials and Methods

Plant materials and sample collection

Hall's panicgrass (*Panicum hallii*, *P. hallii*) genotypes, HAL2 (*P. hallii var. hallii*, upland ecotype) and FIL2 (*P. hallii var. filipes*, lowland ecotype), were grown in a growth chamber at University of Texas at Austin with 26 °C day/ 22 °C night temperature and 12-hr photoperiod. Plants were grown in 3.5 in. square pots with a 6:1:1 mixture of Promix:Turface:Profile soil. The

first fully emerged inflorescence was photographed and used to measure the primary branch number, secondary branch number, and spikelet number as previously described (Wang et al., 2015). The seeds were harvested after maturity and dried at a temperature of 37 °C until the seed weight was stable. The dried seeds were photographed and weighed for the 100-seed weight (mg) value. Phenotypic values are averages from eight replicates showing uniform growth. Young panicle tissues were collected under a dissection microscope and the developmental stages were determined according to the lengths (0.1-0.2 cm for D1 stage, 0.5-1 cm for D2 stage, 4.5-5.5 cm for D3 stage, and 9-11 cm for D4 stage). Tissues for D1 and D2 stage were taken from at least fifty plants and pooled for each biological replicate. Tissues for D3 and D4 stage were taken from at least fifteen plants and pooled for each biological replicate. All samples were harvested at 17:00-18:00 of the day and immediately flash frozen in liquid nitrogen and stored at -80 °C. Three biological replicates from D1 to D4 stages were used for RNA extraction and transcriptome study. Three biological replicates at D1 and D4 stages were used for DNA extraction and methylome study.

Scanning electron microscope

The inflorescences at the D1 and D2 developmental stages were dissected from plants that were collected from the greenhouse at the University of Texas at Austin. These inflorescences were then fixed in a PFA + GA buffer (phosphate-buffered 4% paraformaldehyde + 4% glutaraldehyde, v/v for all solutions) overnight. After removing the unbound fixative, specimens were immersed in 1% OsO4 (osmium tetroxide) overnight followed by the OTOTO method as implemented before (Bess et al., 2005). The specimens were then dehydrated through graded alcohols (50, 70, 90, 95, 100, 100% ethanol, 1:1 HDMS:ethanol (Hexamethyldisilazane:ethanol),

100% HDMS). The air-dried samples were mounted on stubs with adhesive tape and sputter coat and were then imaged in a Zeiss Supra40 SEM-Electron Microscope at 10 kV in the Microscopy and Imaging Facility at the University of Texas at Austin.

Sequence analysis

19,332 one-to-one putative orthologs were identified in a previously published *P. hallii* genomic study (Lovell et al., 2018). The synonymous substitution rates (K_s), non-synonymous rates (K_a) and non-synonymous to synonymous substitution ratios (K_a/K_s) of all one-to-one putative ortholog pairs of HAL2 and FIL2 were estimated by using the "simple Ka/Ks calculator" function from TBtools (Chen et al., 2020).

RNA extraction and RNA-seq library preparation

For RNA preparation, inflorescence samples from four development stages were homogenized to fine powder using a pre-chilled mortar and pestle under liquid nitrogen. Total RNA was isolated using the TRIzol kit (Invitrogen) and samples were treated with DNase I (Invitrogen) to remove contaminating genomic DNA. RNA-Seq libraries were prepared and sequenced in the Department of Energy Joint Genome Institute (Lawrence Berkeley National Laboratory, Berkeley). Briefly, the integrity and concentration of the RNA preparations were checked initially using Nano-Drop (Nano-Drop Technologies) and then by BioAnalyzer (Agilent Technologies). Total RNA-Seq libraries were prepared using Illumina's TruSeq Stranded mRNA HT sample prep kit utilizing poly-A selection of mRNA. Sequencing was performed on the Illumina HiSeq 2500 platform using HiSeq TruSeq SBS sequencing kit, following a 2 × 150 indexed run recipe.

RNA-Seq data analyses

Paired-end RNA-Seq 150-bp reads were quality trimmed ($Q \geq 25$) and reads shorter than 50 bp after trimming were discarded. High-quality filtered reads were aligned to their own reference genomes, *Panicum hallii* HAL v2.1 and *Panicum hallii* v3.1 (https://phytozome-next.jgi.doe.gov/), using GSNAP with a maximum of four mismatches. The HTseq-count was used to generate raw gene counts, and only reads that uniquely mapped to one annotated gene were counted. To filter the genes with low expression and compare the diverged transcriptome assemblies, only one-to-one putative orthologs with counts-per-million above 0.5 (correspond to a count between 8-10 for different library sizes) in at least three samples were retained for further analysis. Principal component analysis and specific gene expression patterns were performed with *vst* normalized expression counts and visualized using the ggplot2 package. Differentially expressed genes with main effects and developmental-specific effects were determined as previously described (Weng et al., 2019). Briefly, to study the additive and interaction effects of genotype and development stage, we determined differential gene expression using statistical testing via likelihood ratio tests in DEseq2 (Love et al., 2014). We used a factorial linear model to test the following: (a) genotype additive effect by comparing the difference in deviance between the two-factor additive model (Genotype + Development stage) and a reduced model (Development stage) formula; (b) the effect across development stages by comparing the difference in deviance between the two-factor additive model (Genotype + Development stage) and a reduced model (Genotype); and (c) interaction effect by comparing the difference in deviance between the full model (Genotype + Development stage + Genotype × Development stage) and an additive reduced model (Genotype + Development stage). Multiple testing was

controlled by *q*-value transformation of likelihood ratio test *p*-value and genes with expression divergence were determined by significant genotype and/or interaction effects (*q*-value < 0.01). To further study developmental stage-specific effects, we conducted a linear model fit to a set of four HAL2-FIL2 contrasts with genes exhibited genotype and/or interaction effects, one at each development stage, through a custom contrast analysis pipeline in DEseq2 with the calculation of $\log_2$-fold change values and adjusted *p*-value (Weng et al., 2019). The *vst* transformed counts of genes were used to plot the divergence expression profiles of putative ortholog pairs between HAL2 and FIL2. The profile of genotype predominant genes with developmental stage-specific information was plotted with the UpSetR package (Conway et al., 2017). The minimum centroid distance was determined with the Mfuzz package (Kumar and M, 2007). The *k*-mean clustering strategy was applied for each category of DEGs and the outputs were visualized using the Complex Heatmap package (Gu et al., 2016). The "GO enrichment" function of TBtools was used to perform the GO enrichment analysis of DEGs in each cluster (Chen et al., 2020).

DNA extraction and bisulfite sequencing library preparation

A CTAB-based protocol was used for DNA extraction from D1 and D4 inflorescence samples of both genotypes (HAL2 and FIL2). The quality of DNA was determined by running on a 1.0 % agarose gel electrophoresis and quantified via Nano-Drop (Nano-Drop Technologies). DNA methylome libraries were prepared from 1ug of genomic DNA and underwent bisulfite treatment using NextFlex Bisulfite-Seq Kit. The resulting bisulfite-converted DNA was PCR- amplified and ligated to adapters, with barcodes. Amplified fragments were purified using the 1.8 × AMPure XP a bead cleaning to remove the small fragments. The libraries were checked for size and concentration using the Agilent Bioanalyzer instrument, followed by sequencing on the

692 Illumina HiSeq 2500 platform at HudsonAlpha Institute.

693

694 **Bisulfite sequencing data analyses**

695 Paired-end bisulfite sequencing 150-bp reads were trimmed using Trim Galore with default
696 options to remove low-quality reads and adaptor sequences. To avoid mapping bias induced by
697 divergent reference genomes, high-quality filtered reads were aligned to their own respective
698 reference genomes, *Panicum hallii* HAL v2.1 and *Panicum hallii* v3.1 (https://phytozome-
699 next.jgi.doe.gov/), using Bismark with options --bowtie2 –bam (Krueger and Andrews, 2011).
700 Reference genomes index files for HAL2 and FIL2 were generated from their corresponding
701 FASTA files using the bismark_genome_preparation function. After removing duplications with
702 the deduplicate_bismark function, BAM output files were sorted in preparation for methylation
703 extraction using Samtools. Genome-wide cytosine reports were obtained using the
704 bismark_methylation_extractor with options -p -ignore 5 -ignore r2 5 -ignore 3prime 2 -ignore
705 3prime r2 -no_overlap –comprehensive -CX. This report was used to generate the read coverage,
706 global methylation level, and distribution of methylation level using ViewBS (Huang et al.,
707 2018). Reads mapped to unmethylated chloroplast genome were used to calculate the frequency
708 of cytosine conversion. For DMRs analysis, only cytosines that were covered by at least five
709 reads were kept for downstream analysis. We studied differential methylation between ecotypes
710 or developmental stages using a genomic feature approach. We defined genomic regions to
711 include promoter regions from 500-bp upstream of the transcription start site, 5'-untranslated
712 regions (5'UTR), protein-coding region (CDS), intron, 3'-untranslated regions (3'UTR), and
713 intergenic regions based on the annotation of gene structure from the existing *P. hallii* genome
714 GFF files for each respective genome. The methylation level in each genomic region was

715 measured as the average of the proportion of all methylated cytosines in that region. The
716 methylation levels of different genomic regions from one-to-one putative orthologs were
717 extracted and used for DMRs analysis. For each DMR contrast, we performed a student *t*-test
718 and calculated the *q*-value using qvalue package to control for the large number of statistical
719 tests. We calculated the methylation changes by subtracting average methylation proportions
720 from HAL2 to FIL2. A cut-off of < 0.01 *q*-value and > 0.1 methylation change were used to
721 identify significant DMRs across five genomic regions and three methylation contexts. In a small
722 number of cases, methylated cytosines were detected for one level of a contrast but not for the
723 other (e.g., methylation was observed in only one ecotype or developmental state for a feature).
724 For these genes/regions we simply used a cut-off > 0.1 methylation proportion change to identify
725 a significant DMRs.
726
727 **Accession numbers**
728 The RNA sequencing data is available at JGI Plant Gene Atlas
729 (https://plantgeneatlas.jgi.doe.gov) (Sreedasyam et al., 2022). The bisulfite sequencing is
730 available in the Sequence Read Archive (SRA) database (https://www.ncbi.nlm.nih.gov/sra/) of
731 NCBI (BioProject ID PRJNA895698). The accession numbers of the major genes mentioned in
732 this paper are provided in Supplemental Table S10.
733
734
735
736
737

Funding information

This research was supported and funded by the National Science Foundation Plant Genome Research Program (IOS-1444533) to T.E.J. The work (proposal: 10.46936/10.25585/60000507) conducted by the U.S. Department of Energy Joint Genome Institute (https://ror.org/04xm1d337), a DOE Office of Science User Facility, is supported by the Office of Science of the U.S. Department of Energy operated under Contract No. DE-AC02-05CH11231.

Acknowledgments

We thank the Department of Energy Joint Genome Institute for permission to publish this analysis using the transcriptome and DNA methylome data of *Panicum hallii*. The scanning electron microscope experiments were performed with the assistance of Michelle Mikesh at the Center for Biomedical Research Support Microscopy and Imaging Facility at the University of Texas at Austin (RRID: SCR_021756) and Dr. Caio Guilherme Pereira from Juenger lab. We

807 thank Shane Merrell, Jason Bonnette, and Ryan Mecredy for growth chambers management and
808 plant materials preparation.
809
810 **Competing interests**
811 The authors declare no competing interests.
812
813 **Figure Legends**
814 **Figure 1. Morphological differences between two representatives of the upland (HAL2) and**
815 **lowland (FIL2) ecotypes in *P. hallii*.**
816 Representative image of the inflorescence (A) and seed (B) morphology of HAL2 and FIL2
817 (Scale bar in A, 1 cm; scale bar in B, 1 mm). (C) Primary branch numbers (PBN), secondary
818 branch numbers (SBN), spikelet numbers (SN), and hundred-seed-weight (HSW, mg) in HAL2
819 and FIL2 plants. In all panels, the bars and error bars are the average values and *SE*, respectively,
820 based on the measurements from eight replicates. The *p*-values were determined by student's t-
821 test.
822
823 **Figure 2. Global transcriptome analysis of gene expression divergence between HAL2 and**
824 **FIL2 inflorescence.**
825 (A) Four stages of inflorescence tissues from HAL2 and FIL2 were collected for RNA-seq.
826 Different stages were designated as D1-D4 according to the lengths of young inflorescences
827 (scale bar, 1 cm) (see method for details). (B) Principal component analysis of the RNA-seq data
828 for the 24 inflorescence samples showing the developmental signatures and genotype effects. (C)
829 Bar plot and Venn diagrams depict genes that are differentially regulated with genotype effects

(Geno) development effects (Devo), and genotype-by-development interaction effects (Int) in factorial linear modeling (q-value < 0.01). Differentially expressed genes with significant genotype and/or interaction effects (red outline labeled) were defined as genes with divergent expression between HAL2 and FIL2 inflorescence.

Figure 3. Stage-specific contrast of interaction genes during inflorescence development.

(A) Quantification of stage-specific expression of interaction genes as HAL2 predominant (red bar on the top), FIL2 predominant (blue bar on the top), and rank changing (grey bar on the top) patterns. The numbers of genes showing developmental-specific expression patterns in one or more of sampling stages are shown in black vertical bars of the figure. Black dots at the bottom of each vertical bar indicate the developmental-specific expression identified at each sampling stage. The lined dots indicate two or more sampling stages showing differential expression between two genotypes. (B) Expression of interaction genes with the HAL2 predominant (upper), FIL2 predominant (middle), and rank changing patterns (bottom). The *x*-axis represents four developmental stages, while the *y*-axis represents normalized counts using variance stabilizing transformation in DEseq2. In all panels, the points and error bars are the average values and *SE*, respectively, based on normalized counts of three RNA-seq replicates. The gene ID and the names of their putative orthologs are shown on the top of the expression pattern plots.

Figure 4. Divergence patterns of interaction genes during inflorescence development.

(A) Heatmaps of gene expression with interaction genes between HAL2 and FIL2 across four developmental stages. Only gene expression data from 5,078 interaction genes are used for clustering. The minimum centroid distance was used to determine the number of cluster cores.

The genotype and development information is added on top as color bars. (B) The dot plot of the most significantly enriched Gene Ontology (GO) terms from each cluster (*y*-axis) in 5,078 interaction genes. The size of the dots represents the number of genes in the significant differentially expressed gene list associated with the GO term and the color of the dots represents the False Discovery Rate (FDR) corrected *p*-value (Benjamini-Hochberg method). (C) Expression of genes from the enriched GO term of "response to cytokinin" (GO:0009735). The *x*-axis represents four developmental stages, while the *y*-axis represents normalized counts using variance stabilizing transformation in DEseq2. In all panels, the points and error bars are the average values and *SE*, respectively, based on normalized counts of three RNA-seq replicates. The gene ID and the names of their putative orthologs are shown on the top of the expression pattern plots.

Figure 5. Global DNA methylation profiling and influence of DNA methylation on gene expression during inflorescence development.

(A) The distribution of CG, CHG, and CHH methylation levels (mean values of three biological replicates) and gene density across the HAL2 and FIL2 chromosomes from D1 inflorescence. (B) DNA Methylation levels in different inflorescence tissues and genotypes. The bars and error bars are the average values and *SE*. *P*-values less than 0.05 are labeled as asterisks (student's t-test). (C) Methylation level within gene body and 2 kb flanking regions in CG, CHG, and CHH contexts for the gene sets that are expressed at different levels in HAL2 and FIL2 from D1 inflorescence. The average of three replicates was displayed for CG, CHG, and CHH contexts. The data for the D4 stage of inflorescences are given in Supplemental Figure S10 and S12.

Figure 6. Differential DNA methylation regions between HAL2 and FIL2 inflorescences.

(A) Pairwise comparisons of methylation levels from one-to-one putative ortholog pairs between HAL2 and FIL2 D1 inflorescence in CG, CHG, and CHH contexts across five different genomic features. Blue dots represent genes with significant hypermethylation in FIL2, while red dots represent genes with significant hypermethylation in HAL2. Grey dots represent genes with no significant methylation difference. (B) Number of differentially methylated genes between HAL2 and FIL2 D1 inflorescence in CG, CHG, and CHH contexts across five different genomic features are shown in bar plots. The total number of differentially methylated genes in each context is shown in the associated pie chart. In the pie charts, "NS" refers to non-significant methylation difference, while "Sig" refers to significant methylation difference (A cut-off of < 0.01 *q*-value and > 0.1 methylation change were used to identify significant methylation difference). The data for the comparison between HAL2 and FIL2 at D4 inflorescence is given in Supplemental Figure S13. The comparison between D1 and D4 inflorescence in both HAL2 or FIL2 background are given in Supplemental Figure S16.

Figure 7. Association of differentially methylated genes with differentially expressed genes.

Venn diagrams depicting the number of differentially expressed genes (yellow circle, DEGs) and differentially methylated regions (DMRs)-associated genes (blue circle, DMRs) between HAL2 and FIL2 D1 inflorescence in CG (A), CHG (B), and CHH (C) contexts across five different genomic features. Two-dimensional scatter plots depict the association of differentially expressed genes and differentially methylated regions in CG (A), CHG (B), and CHH (C) contexts across five different genomic features. The *x*-axis represents relative gene expression change (log2fold change), while the *y*-axis represents relative methylation change (HAL2 subtracted from FIL2).

The data for the association of differentially methylated genes with differentially expressed genes at D4 inflorescence are given in Supplemental Figure S18.

Figure 8. Evolution of differentially methylated regions-associated differentially expressed gene pairs.

(A) and (B) The K_a/K_s values distribution of gene pairs from differentially methylated regions (DMRs)-associated differentially expressed genes DEGs and one-to-one putative orthologs between HAL2 and FIL2. (A) The mean values are indicated by the dashed line. (B) The solid black line marks $K_a/K_s = 1$. The red dots mark the DMRs-associated DEGs with K_a/K_s ratio larger than 1, while the blue dots mark the DMRs-associated DEGs with K_a/K_s ratio less than 1. The grey dots represent all one-to-one putative orthologs. (C) Differential methylation patterns of CG, CHG, and CHH contexts across five different genomic features for DMRs-associated DEGs genes that are putatively positively selected. In all panels, the bar plots and error bars are the average values and *SE*, respectively, based on methylation level from three replicates. (D) Expression patterns of DMRs-associated DEGs genes that are putatively positively selected. The *x*-axis represents four developmental stages, while the *y*-axis represents normalized counts using variance stabilizing transformation in DEseq2. In all panels, the points and error bars are the average values and *SE*, respectively, based on normalized counts of three RNA-seq replicates.

References

Ashikari M, Sakakibara H, Lin SY, Yamamoto T, Takashi T, Nishimura A, Angeles ER, Qian Q, Kitano H, Matsuoka M (2005) Cytokinin oxidase regulates rice grain production. Science **309**: 741-745

922 **Barazesh S, McSteen P** (2008) Hormonal control of grass inflorescence development. Trends
923 Plant Sci **13**: 656-662
924 **Bartrina I, Otto E, Strnad M, Werner T, Schmulling T** (2011) Cytokinin regulates the
925 activity of reproductive meristems, flower organ size, ovule formation, and thus seed
926 yield in *Arabidopsis thaliana*. Plant Cell **23**: 69-80
927 **Bess EC, Doust AN, Kellogg EA** (2005) A naked grass in the "bristle clade": a phylogenetic and
928 developmental study of *Panicum* section *Bulbosa* (Paniceae : Poaceae). Int J Plant Sci
929 **166**: 371-381
930 **Bewick AJ, Schmitz RJ** (2017) Gene body DNA methylation in plants. Curr Opin Plant Biol **36**:
931 103-110
932 **Bolduc N, Hake S** (2009) The maize transcription factor KNOTTED1 directly regulates the
933 gibberellin catabolism gene *ga2ox1*. Plant Cell **21**: 1647- 1658
934 **Bouche N, Lauressergues D, Gasciolli V, Vaucheret H** (2006) An antagonistic function for
935 *Arabidopsis* DCL2 in development and a new function for DCL4 in generating viral
936 siRNAs. EMBO J **25**: 3347-3356
937 **Buendia-Monreal M, Gillmor CS** (2018) The times they are a-changin': heterochrony in plant
938 development and evolution. Front Plant Sci **9**: 1349
939 **Chan SW, Henderson IR, Jacobsen SE** (2005) Gardening the genome: DNA methylation in
940 *Arabidopsis thaliana*. Nat Rev Genet **6**: 351-360
941 **Chen CJ, Chen H, Zhang Y, Thomas HR, Frank MH, He YH, Xia R** (2020) TBtools: an
942 integrative toolkit developed for interactive analyses of big biological data. Mol Plant **13**:
943 1194-1202

Conway JR, Lex A, Gehlenborg N (2017) UpSetR: an R package for the visualization of intersecting sets and their properties. Bioinformatics **33**: 2938-2940

Dai XH, Liu ZH, Qiao M, Li J, Li S, Xiang FN (2017) ARR12 promotes *de novo* shoot regeneration in *Arabidopsis thaliana* via activation of *WUSCHEL* expression. J Integr Plant Biol **59**: 747-758

Deveshwar P, Prusty A, Sharma S, Tyagi AK (2020) Phytohormone-mediated molecular mechanisms involving multiple genes and QTL govern grain number in rice. Front Genet **11**: 586462

Eveland AL, Goldshmidt A, Pautler M, Morohashi K, Liseron-Monfils C, Lewis MW, Kumari S, Hiraga S, Yang F, Unger-Wallace E, Olson A, Hake S, Vollbrecht E, Grotewold E, Ware D, Jackson D (2014) Regulatory modules controlling maize inflorescence architecture. Genome Res **24**: 431-443

Feng N, Song GY, Guan JT, Chen K, Jia ML, Huang DH, Wu JJ, Zhang LC, Kong XY, Geng SF, Liu J, Li AL, Mao L (2017) Transcriptome profiling of wheat inflorescence development from spikelet initiation to floral patterning identified stage-specific regulatory genes. Plant Physiol **174**: 1779-1794

Fernandez-Nohales P, Domenech MJ, Martinez de Alba AE, Micol JL, Ponce MR, Madueno F (2014) AGO1 controls arabidopsis inflorescence architecture possibly by regulating *TFL1* expression. Ann Bot **114**: 1471-1481

Furutani I, Sukegawa S, Kyozuka J (2006) Genome-wide analysis of spatial and temporal gene expression in rice panicle development. Plant J **46**: 503-511

Gould BA, Palacio-Mejia JD, Jenkins J, Mamidi S, Barry K, Schmutz J, Juenger TE, Lowry DB (2018) Population genomics and climate adaptation of a C_4 perennial grass, *Panicum hallii* (Poaceae). BMC Genomics **19**: 792

Gu ZG, Eils R, Schlesner M (2016) Complex heatmaps reveal patterns and correlations in multidimensional genomic data. Bioinformatics **32**: 2847-2849

Harder LD, Prusinkiewicz P (2013) The interplay between inflorescence development and function as the crucible of architectural diversity. Ann Bot **112**: 1477-1493

Harrop TW, Ud Din I, Gregis V, Osnato M, Jouannic S, Adam H, Kater MM (2016) Gene expression profiling of reproductive meristem types in early rice inflorescences by laser microdissection. Plant J **86**: 75-88

Higo A, Saihara N, Miura F, Higashi Y, Yamada M, Tamaki S, Ito T, Tarutani Y, Sakamoto T, Fujiwara M, Kurata T, Fukao Y, Moritoh S, Terada R, Kinoshita T, Ito T, Kakutani T, Shimamoto K, Tsuji H (2020) DNA methylation is reconfigured at the onset of reproduction in rice shoot apical meristem. Nat Commun **11**: 4079

Huang H, Liu RE, Niu QF, Tang K, Zhang B, Zhang H, Chen KS, Zhu JK, Lang ZB (2019) Global increase in DNA methylation during orange fruit development and ripening. Proc Natl Acad Sci USA **116**: 1430-1436

Huang XS, Zhang SL, Li KQ, Thimmapuram J, Xie SJ, Wren J (2018) ViewBS: a powerful toolkit for visualization of high-throughput bisulfite sequencing data. Bioinformatics **34**: 708-709

Jia SZ, Xiong YF, Xiao PP, Wang X, Yao JL (2019) OsNF-YC10, a seed preferentially expressed gene regulates grain width by affecting cell proliferation in rice. Plant Sci **280**: 219-227

Kawakatsu T, Huang SC, Jupe F, Sasaki E, Schmitz RJ, Urich MA, Castanon R, Nery JR, Barragan C, He Y, Chen H, Dubin M, Lee CR, Wang C, Bemm F, Becker C, O'Neil R, O'Malley RC, Quarless DX, Genomes C, Schork NJ, Weigel D, Nordborg M, Ecker JR (2016) Epigenomic diversity in a global collection of *Arabidopsis thaliana* accessions. Cell **166**: 492-505

Kellogg EA, Camara PEAS, Rudall PJ, Ladd P, Malcomber ST, Whipple CJ, Doust AN (2013) Early inflorescence development in the grasses (Poaceae). Front Plant Sci **4**: 250

Kellogg EA (2022) Genetic control of branching patterns in grass inflorescences. Plant Cell **34**: 2518-2533

Khasanova A, Lovell JT, Bonnette J, Weng XY, Jenkins J, Yoshinaga Y, Schmutz J, Juenger TE (2019) The genetic architecture of shoot and root trait divergence between mesic and xeric ecotypes of a perennial grass. Front Plant Sci **10**: 366

Koo BH, Yoo SC, Park JW, Kwon CT, Lee BD, An G, Zhang ZY, Li JJ, Li ZC, Paek NC (2013) Natural variation in *OsPRR37* regulates heading date and contributes to rice cultivation at a wide range of latitudes. Mol Plant **6**: 1877-1888

Krueger F, Andrews SR (2011) Bismark: a flexible aligner and methylation caller for Bisulfite-Seq applications. Bioinformatics **27**: 1571-1572

Kumar L, M EF (2007) Mfuzz: a software package for soft clustering of microarray data. Bioinformation **2**: 5-7

Kurakawa T, Ueda N, Maekawa M, Kobayashi K, Kojima M, Nagato Y, Sakakibara H, Kyozuka J (2007) Direct control of shoot meristem activity by a cytokinin-activating enzyme. Nature **445**: 652-655

Kyozuka J, Tokunaga H, Yoshida A (2014) Control of grass inflorescence form by the fine-tuning of meristem phase change. Curr Opin Plant Biol **17**: 110-115

Law JA, Jacobsen SE (2010) Establishing, maintaining and modifying DNA methylation patterns in plants and animals. Nat Rev Genet **11**: 204-220

Lee DY, Lee J, Moon S, Park SY, An G (2007) The rice heterochronic gene *SUPERNUMERARY BRACT* regulates the transition from spikelet meristem to floral meristem. Plant J **49**: 64-78

Li X, Zhu JD, Hu FY, Ge S, Ye MZ, Xiang H, Zhang GJ, Zheng XM, Zhang HY, Zhang SL, Li Q, Luo RB, Yu C, Yu J, Sun JF, Zou XY, Cao XF, Xie XF, Wang J, Wang W (2012) Single-base resolution maps of cultivated and wild rice methylomes and regulatory roles of DNA methylation in plant gene expression. BMC Genomics **13**: 300

Li ZQ, Tang MQ, Luo DJ, Kashif MH, Cao S, Zhang WX, Hu YL, Huang Z, Yue J, Li R, Chen P (2021) Integrated methylome and transcriptome analyses reveal the molecular mechanism by which DNA methylation regulates Kenaf flowering. Front Plant Sci **12**: 709030

Liao PF, Ouyang JX, Zhang JJ, Yang L, Wang X, Peng XJ, Wang D, Zhu YL, Li SB (2019) OsDCL3b affects grain yield and quality in rice. Plant Mol Biol **99**: 193-204

Liu C, Teo ZW, Bi Y, Song SY, Xi WY, Yang XB, Yin ZC, Yu H (2013) A conserved genetic pathway determines inflorescence architecture in *Arabidopsis* and rice. Dev Cell **24**: 612-622

Love MI, Huber W, Anders S (2014) Moderated estimation of fold change and dispersion for RNA-seq data with DESeq2. Genome Biol **15**: 550

Lovell JT, Jenkins J, Lowry DB, Mamidi S, Sreedasyam A, Weng XY, Barry K, Bonnette J, Campitelli B, Daum C, Gordon SP, Gould BA, Khasanova A, Lipzen A, MacQueen A, Palacio-Mejia JD, Plott C, Shakirov EV, Shu SQ, Yoshinaga Y, Zane M, Kudrna D, Talag JD, Rokhsar D, Grimwood J, Schmutz J, Juenger TE (2018) The genomic landscape of molecular responses to natural drought stress in *Panicum hallii*. Nat Commun **9**: 5213

Lovell JT, Schwartz S, Lowry DB, Shakirov EV, Bonnette JE, Weng XY, Wang M, Johnson J, Sreedasyam A, Plott C, Jenkins J, Schmutz J, Juenger TE (2016) Drought responsive gene expression regulatory divergence between upland and lowland ecotypes of a perennial C_4 grass. Genome Res **26**: 510-518

Lowry DB, Hernandez K, Taylor SH, Meyer E, Logan TL, Barry KW, Chapman JA, Rokhsar DS, Schmutz J, Juenger TE (2015) The genetics of divergence and reproductive isolation between ecotypes of *Panicum hallii*. New Phytol **205**: 402-414

Martin GT, Seymour DK, Gaut BS (2021) CHH methylation islands: a nonconserved feature of grass genomes that is positively associated with transposable elements but negatively associated with gene-body methylation. Genome Biol Evol **13**: evab144

Moritoh S, Eun CH, Ono A, Asao H, Okano Y, Yamaguchi K, Shimatani Z, Koizumi A, Terada R (2012) Targeted disruption of an orthologue of *DOMAINS REARRANGED METHYLASE 2*, *OsDRM2*, impairs the growth of rice plants by abnormal DNA methylation. Plant J **71**: 85-98

Niederhuth CE, Bewick AJ, Ji L, Alabady MS, Kim KD, Li Q, Rohr NA, Rambani A, Burke JM, Udall JA, Egesi C, Schmutz J, Grimwood J, Jackson SA, Springer NM,

Schmitz RJ (2016) Widespread natural variation of DNA methylation within angiosperms. Genome Biol **17**: 194

Palacio-Mejia JD, Grabowski PP, Ortiz EM, Silva-Arias GA, Haque T, Des Marais DL, Bonnette J, Lowry DB, Juenger TE (2021) Geographic patterns of genomic diversity and structure in the C_4 grass *Panicum hallii* across its natural distribution. AoB Plants **13**: plab002

Parvathaneni RK, Bertolini E, Shamimuzzaman M, Vera DL, Lung PY, Rice BR, Zhang JF, Brown PJ, Lipka AE, Bass HW, Eveland AL (2020) The regulatory landscape of early maize inflorescence development. Genome Biol **21**: 165

Rajkumar MS, Gupta K, Khemka NK, Garg R, Jain M (2020) DNA methylation reprogramming during seed development and its functional relevance in seed size/weight determination in chickpea. Commun Biol **3**: 340

Rao NN, Prasad K, Kumar PR, Vijayraghavan U (2008) Distinct regulatory role for RFL, the rice LFY homolog, in determining flowering time and plant architecture. Proc Natl Acad Sci U S A **105**: 3646-3651

Razzaque S, Juenger TE (2022) The ecology and quantitative genetics of seed and seedling traits in upland and lowland ecotypes of a perennial grass. Evol Lett **6**: 460-473

Sadras VO (2007) Evolutionary aspects of the trade-off between seed size and number in crops. Field Crops Res **100:** 125-138

Shi Y, Zhang XT, Chang XJ, Yan MK, Zhao HM, Qin Y, Wang HF (2021) Integrated analysis of DNA methylome and transcriptome reveals epigenetic regulation of CAM photosynthesis in pineapple. BMC Plant Biol **21**: 19

Sreedasyam A, Plott C, Hossain MS, Lovell JT, Grimwood J, Jenkins JW, Daum C, Barry K, Carlson J, Shu SQ, Phillips J, Amirebrahimi M, Zane M, Wang M, Goodstein D, Haas FB, Hiss M, Perroud P-F, Jawdy SS, Hu R, Johnson J, Kropat J, Gallaher SD, Lipzen A, Tillman R, Shakirov EV, Weng XY, Torres-Jerez I, Weers B, Conde D, Pappas MR, Liu LF, Muchlinski A, Jiang H, Shyu C, Huang P, Sebastian J, Laiben C, Medlin A, Carey S, Carrell AA, Perales M, Swaminathan K, Allona I, Grattapaglia D, Cooper EA, Tholl D, Vogel JP, Weston DJ, Yang XH, Brutnell TP, Kellogg EA, Baxter I, Udvardi M, Tang YH, Mockler TC, Juenger TE, Mullet J, Rensing SA, Tuskan GA, Merchant SS, Stacey G, Schmutz J (2022) JGI Plant Gene Atlas: An updateable transcriptome resource to improve structural annotations and functional gene descriptions across the plant kingdom. BioRxiv: 2022.09.30.510380

Sun YH, Dong L, Zhang Y, Lin D, Xu WZ, Ke CX, Han LQ, Deng LL, Li GL, Jackson D, Li XW, Yang F (2020) 3D genome architecture coordinates *trans* and *cis* regulation of differentially expressed ear and tassel genes in maize. Genome Biol **21**: 143

Tate PH, Bird AP (1993) Effects of DNA methylation on DNA-binding proteins and gene expression. Curr Opin Genet Dev **3**: 226-231

Teo ZWN, Song SY, Wang YQ, Liu J, Yu H (2014) New insights into the regulation of inflorescence architecture. Trends in Plant Sci **19**: 158-165

Tu CW, Li TT, Liu XY (2019) Genetic and epigenetic regulatory mechanism of rice panicle development. 2018 International Conference on Biotechnology and Bioengineering (8th Icbb) **2079**: 020001

Wang L, Sun SY, Jin JY, Fu DB, Yang XF, Weng XY, Xu CG, Li XH, Xiao JH, Zhang QF (2015) Coordinated regulation of vegetative and reproductive branching in rice. Proc Natl Acad Sci USA **112**: 15504-15509

Wang L, Xie WB, Chen Y, Tang WJ, Yang JY, Ye RJ, Liu L, Lin YJ, Xu CG, Xiao JH, Zhang QF (2010) A dynamic gene expression atlas covering the entire life cycle of rice. Plant J **61**: 752-766

Weng XY, Lovell JT, Schwartz SL, Cheng CD, Haque T, Zhang L, Razzaque S, Juenger TE (2019) Complex interactions between day length and diurnal patterns of gene expression drive photoperiodic responses in a perennial C_4 grass. Plant Cell Environ **42**: 2165-2182

Wulfridge P, Langmead B, Feinberg AP, Hansen KD (2019) Analyzing whole genome bisulfite sequencing data from highly divergent genotypes. Nucleic Acids Res **47**: e117

Xu G, Lyu J, Li Q, Liu H, Wang DF, Zhang M, Springer NM, Ross-Ibarra J, Yang JL (2020) Evolutionary and functional genomics of DNA methylation in maize domestication and improvement. Nat Commun **11**: 5539

Yan WH, Liu HY, Zhou XC, Li QP, Zhang J, Lu L, Liu TM, Liu HJ, Zhang CJ, Zhang ZY, Shen GJ, Yao W, Chen HX, Yu SB, Xie WB, Xing YZ (2013) Natural variation in *Ghd7.1* plays an important role in grain yield and adaptation in rice. Cell Res **23**: 969-971

Yang HX, Chang F, You CJ, Cui J, Zhu GF, Wang L, Zheng Y, Qi J, Ma H (2015) Whole-genome DNA methylation patterns and complex associations with gene structure and expression during flower development in *Arabidopsis*. Plant J **81**: 268-281

Zhang DB, Yuan Z (2014) Molecular control of grass inflorescence development. Annu Rev Plant Biol **65**: 553-578

Zhang H, Zhu SS, Liu TZ, Wang CM, Cheng ZJ, Zhang X, Chen LP, Sheng PK, Cai MH, Li CN, Wang JC, Zhang Z, Chai JT, Zhou L, Lei CL, Guo XP, Wang JL, Wang J, Jiang L, Wu CY, Wan JM (2019) DELAYED HEADING DATE1 interacts with OsHAP5C/D, delays flowering time and enhances yield in rice. Plant Biotechnol J **17**: 531-539

Zhang HM, Lang ZB, Zhu JK (2018) Dynamics and function of DNA methylation in plants. Nat Rev Mol Cell Biol **19**: 489-506

Zhang L, Yu H, Ma B, Liu GF, Wang JJ, Wang JM, Gao RC, Li JJ, Liu JY, Xu J, Zhang YY, Li Q, Huang XH, Xu JL, Li JM, Qian Q, Han B, He ZH, Li JY (2017) A natural tandem array alleviates epigenetic repression of *IPA1* and leads to superior yielding rice. Nat Commun **8**: 14789

Zhu CM, Yang J, Box MS, Kellogg EA, Eveland AL (2018) A dynamic co-expression map of early inflorescence development in *Setaria viridis* provides a resource for gene discovery and comparative genomics. Front Plant Sci **9**: 1309

Zhu ZF, Tan LB, Fu YC, Liu FX, Cai HW, Xie DX, Wu F, Wu JZ, Matsumoto T, Sun CQ (2013) Genetic control of inflorescence architecture during rice domestication. Nat Commun **4**: 2200

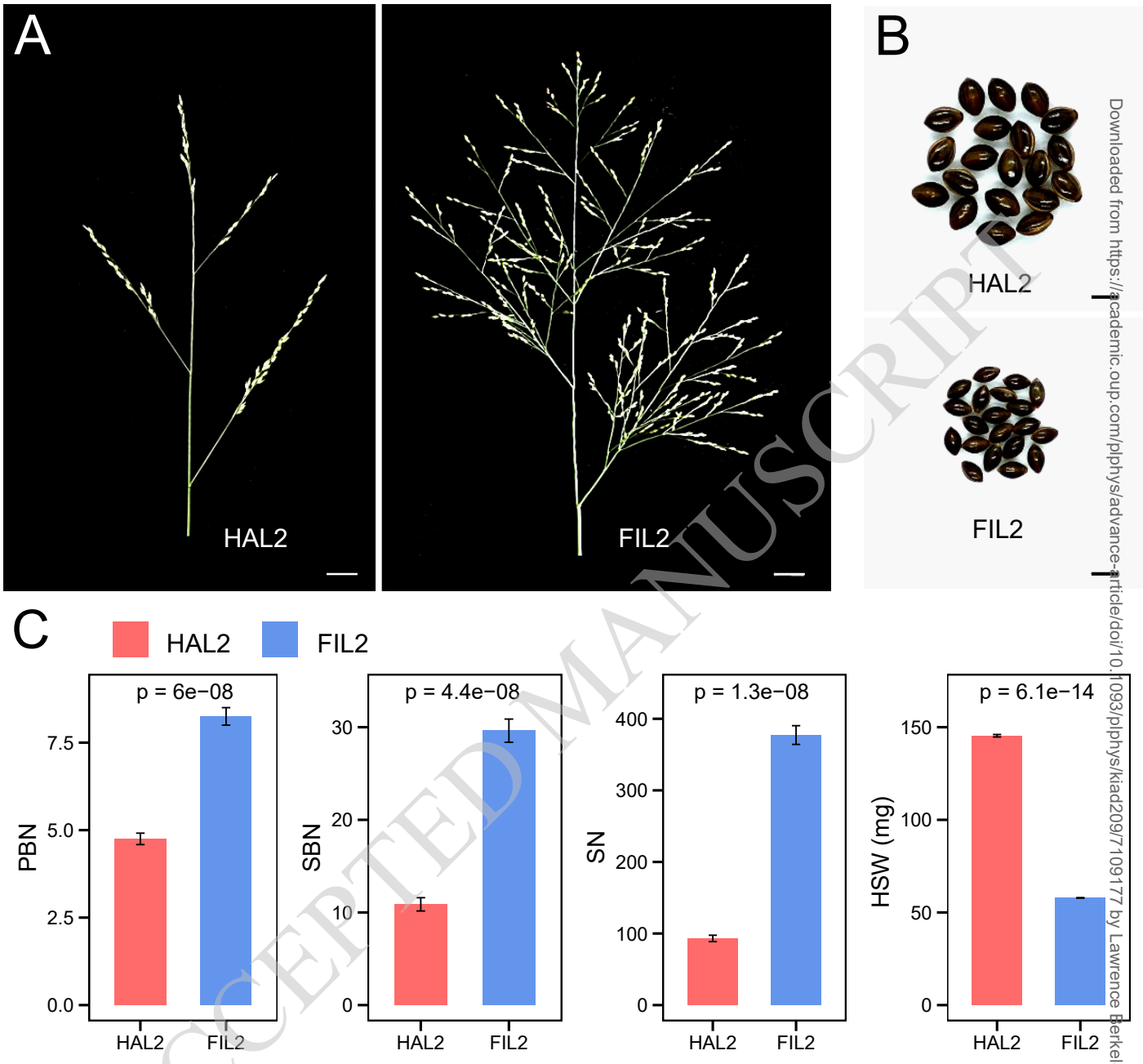

Figure 1. Morphological differences between two representatives of the upland (HAL2) and lowland (FIL2) ecotypes in *P. hallii*.

Representative image of the inflorescence (A) and seed (B) morphology of HAL2 and FIL2 (Scale bar in A, 1 cm; scale bar in B, 1 mm). (C) Primary branch numbers (PBN), secondary branch numbers (SBN), spikelet numbers (SN), and hundred-seed-weight (HSW, mg) in HAL2 and FIL2 plants. In all panels, the bars and error bars are the average values and *SE*, respectively, based on the measurements from eight replicates. The *p*-values were determined by student's t-test.

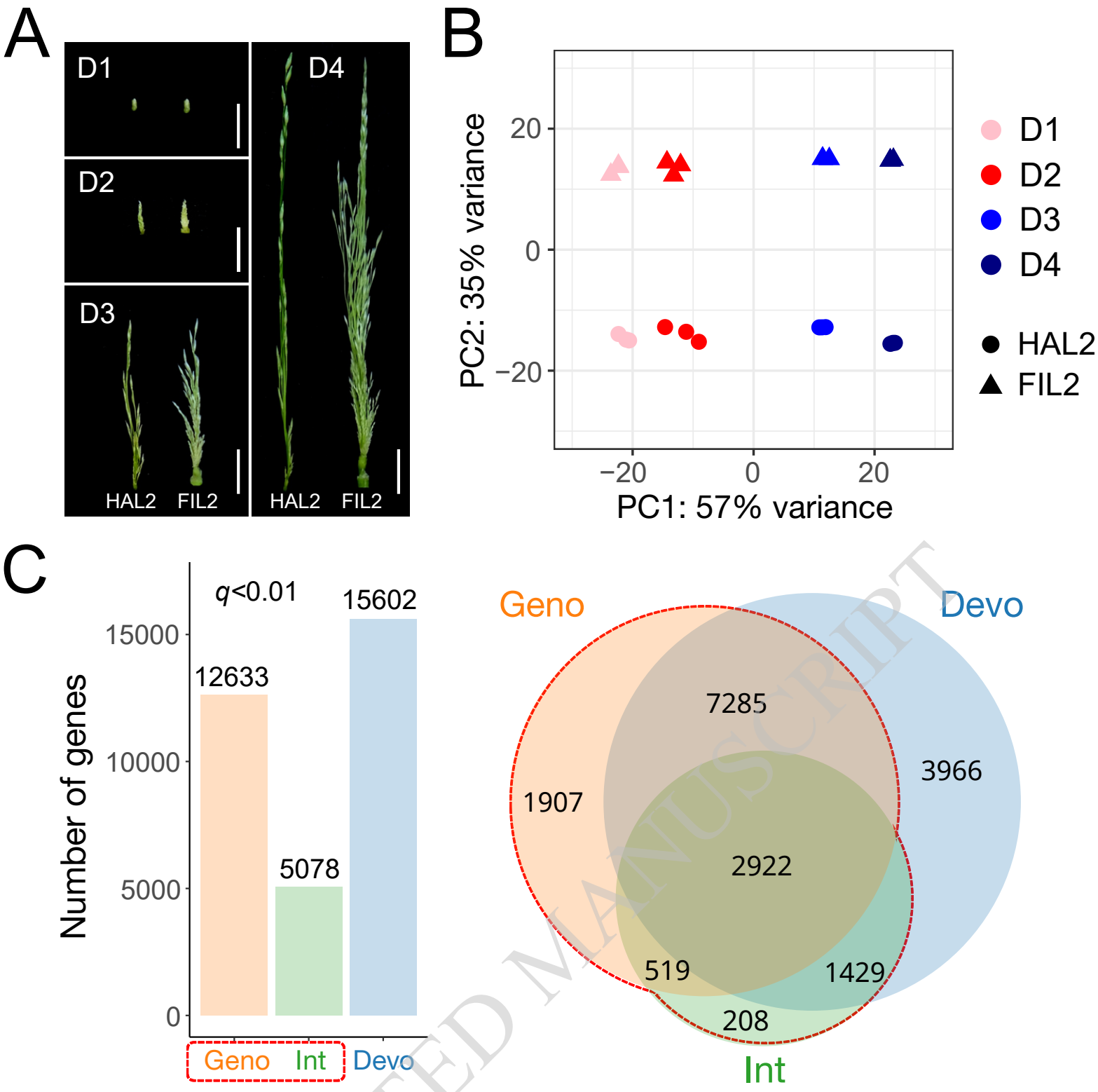

Figure 2. Global transcriptome analysis of gene expression divergence between HAL2 and FIL2 inflorescence.

(A) Four stages of inflorescence tissues from HAL2 and FIL2 were collected for RNA-seq. Different stages were designated as D1-D4 according to the lengths of young inflorescences (scale bar, 1 cm) (see method for details). (B) Principal component analysis of the RNA-seq data for the 24 inflorescence samples showing the developmental signatures and genotype effects. (C) Bar plot and venn diagrams depict genes that are differentially regulated with genotype effects (Geno) development effects (Devo), and genotype-by-development interaction effects (Int) in factorial linear modeling (q-value < 0.01). Differentially expressed genes with significant genotype and/or interaction effects (red outline labeled) were defined as genes with divergent expression between HAL2 and FIL2 inflorescence.

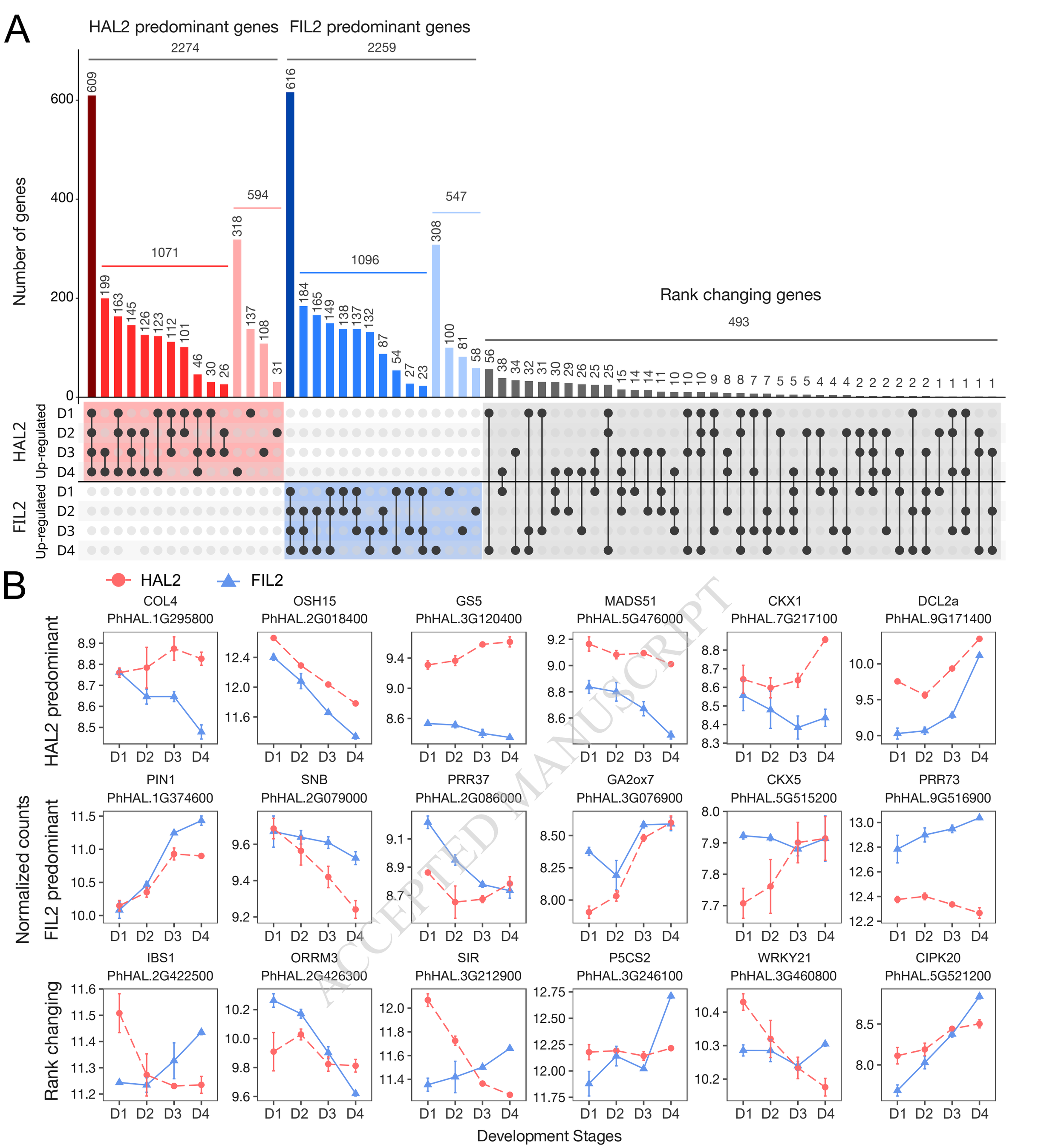

Figure 3. Stage-specific contrast of interaction genes during inflorescence development.

(A) Quantification of stage-specific expression of interaction genes as HAL2 predominant (red bar on the top), FIL2 predominant (blue bar on the top), and rank changing (grey bar on the top) patterns. The numbers of genes showing developmental-specific expression patterns in one or more of sampling stages are shown in black vertical bars of the figure. Black dots at the bottom of each vertical bar indicate the developmental-specific expression identified at each sampling stage. The lined dots indicate two or more sampling stages showing differential expression between two genotypes.
(B) Expression of interaction genes with the HAL2 predominant (upper), FIL2 predominant (middle), and rank changing patterns (bottom). The *x*-axis represents four developmental stages, while the *y*-axis represents normalized counts using variance stabilizing transformation in DEseq2. In all panels, the points and error bars are the average values and *SE*, respectively, based on normalized counts of three RNA-seq replicates. The gene ID and the names of their putative orthologs are shown on the top of the expression pattern plots.

Figure 4. Divergence patterns of interaction genes during inflorescence development.
(A) Heatmaps of gene expression with interaction genes between HAL2 and FIL2 across four developmental stages. Only gene expression data from 5,078 interaction genes are used for clustering. The minimum centroid distance was used to determine the number of cluster cores. The genotype and development information is added on top as color bars. (B) The dot plot of the most significantly enriched Gene Ontology (GO) terms from each cluster (*y*-axis) in 5,078 interaction genes. The size of the dots represents the number of genes in the significant differentially expressed gene list associated with the GO term and the color of the dots represents the False Discovery Rate (FDR) corrected *p*-values (Benjamini-Hochberg method). (C) Expression of genes from the enriched GO term of "response to cytokinin" (GO:0009735). The *x*-axis represents four developmental stages, while the *y*-axis represents normalized counts using variance stabilizing transformation in DEseq2. In all panels, the points and error bars are the average values and *SE*, respectively, based on normalized counts of three RNA-seq replicates. The gene ID and the names of their putative orthologs are shown on the top of the expression pattern plots.

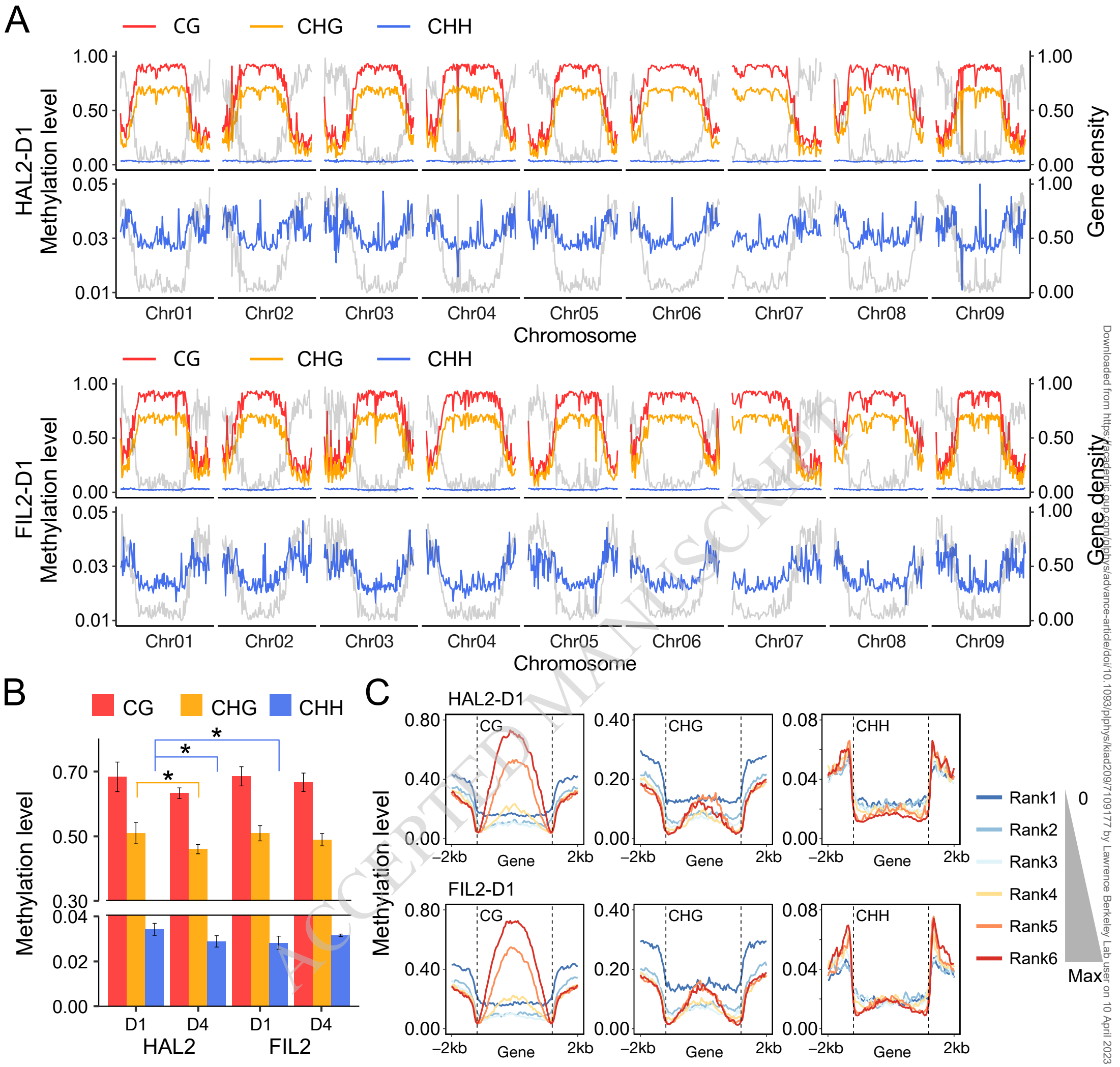

Figure 5. Global DNA methylation profiling and influence of DNA methylation on gene expression during inflorescence development.

(A) The distribution of CG, CHG, and CHH methylation levels (mean values of three biological replicates) and gene density across the HAL2 and FIL2 chromosomes from D1 inflorescence. (B) DNA Methylation levels in different inflorescence tissues and genotypes. The bars and error bars are the average values and *SE*. *P*-values less than 0.05 were labeled as asterisks (student's t-test). (C) Methylation level within gene body and 2 kb flanking regions in CG, CHG, and CHH contexts for the gene sets that are expressed at different levels in HAL2 and FIL2 from D1 inflorescence. The average of three replicates was displayed for CG, CHG, and CHH contexts. The data for the D4 stage of inflorescences are given in Supplemental Figure S10 and S12.

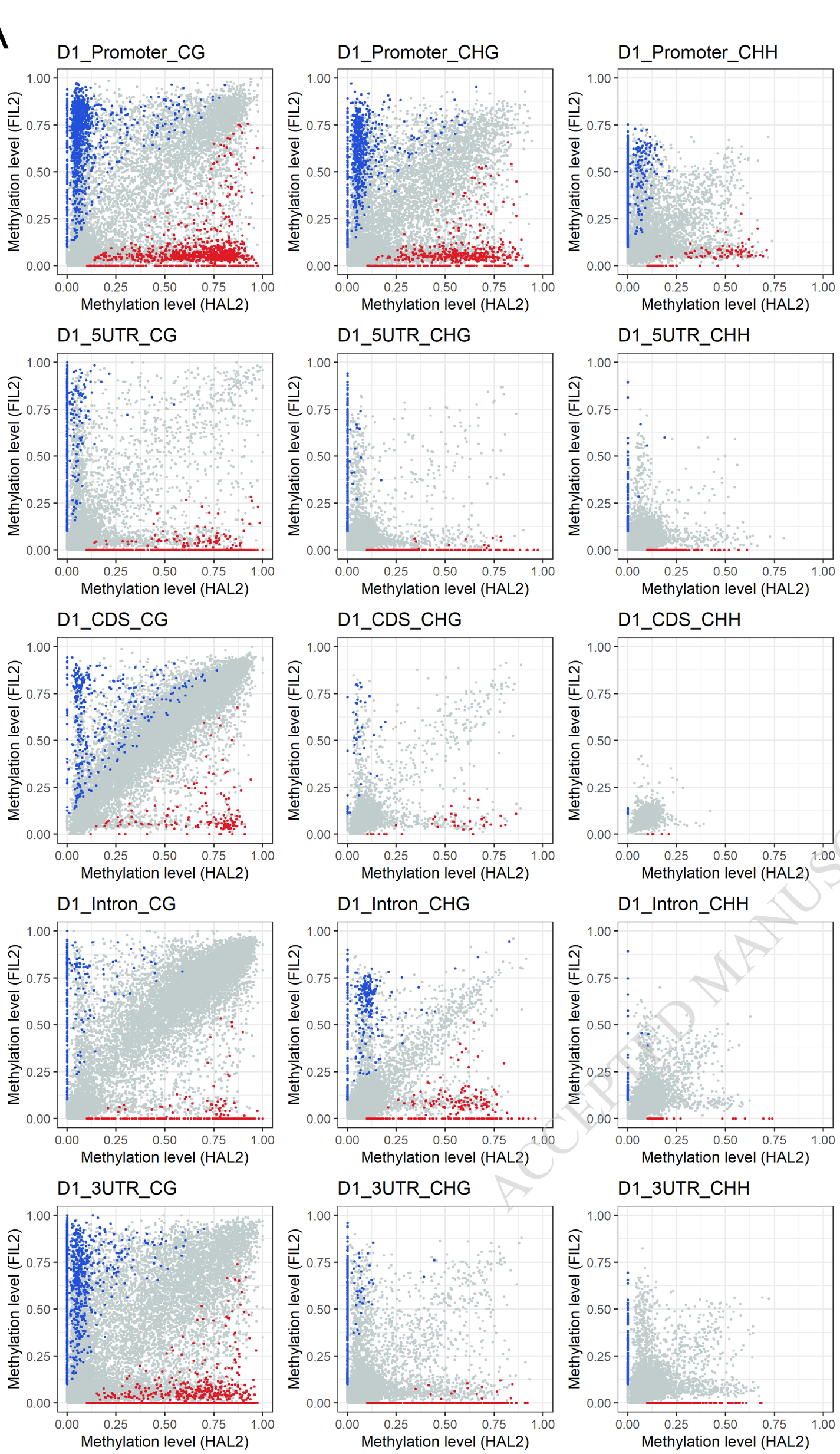

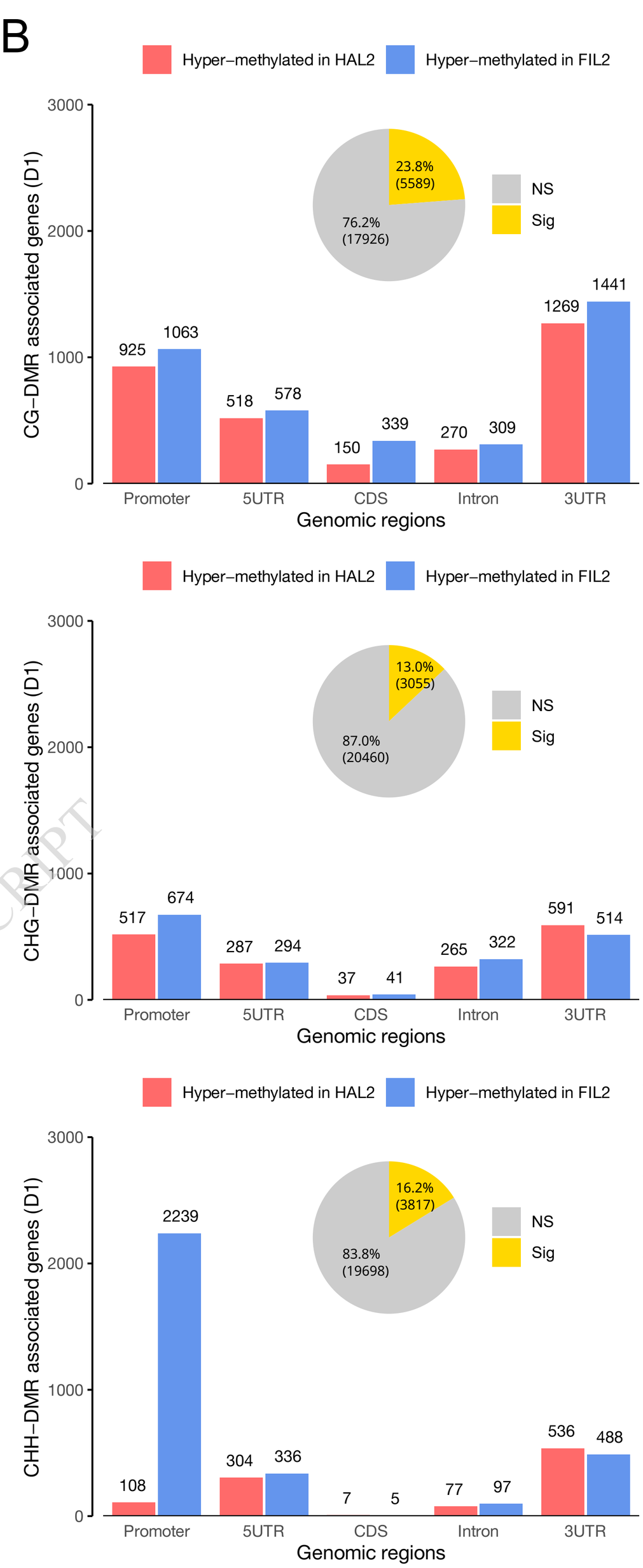

Figure 6. Differential DNA methylation regions between HAL2 and FIL2 inflorescences.

(A) Pairwise comparisons of methylation levels from one-to-one putative ortholog pairs between HAL2 and FIL2 D1 inflorescence in CG, CHG, and CHH contexts across five different genomic features. Blue dots represent genes with significant hypermethylation in FIL2, while red dots represent genes with significant hypermethylation in HAL2. Grey dots represent genes with no significant methylation difference. (B) Number of differentially methylated genes between HAL2 and FIL2 D1 inflorescence in CG, CHG, and CHH contexts across five different genomic features are shown in bar plots. The total number of differentially methylated genes in each context is shown in the associated pie chart. In the pie charts, "NS" refers to non-significant methylation difference, while "Sig" refers to significant methylation difference (A cut-off of < 0.01 *q*-value and > 0.1 methylation change were used to identify significant methylation difference). The data for the comparison between HAL2 and FIL2 at D4 inflorescence is given in Supplemental Figure S13. The comparison between D1 and D4 inflorescence in both HAL2 or FIL2 background are given in Supplemental Figure S16.

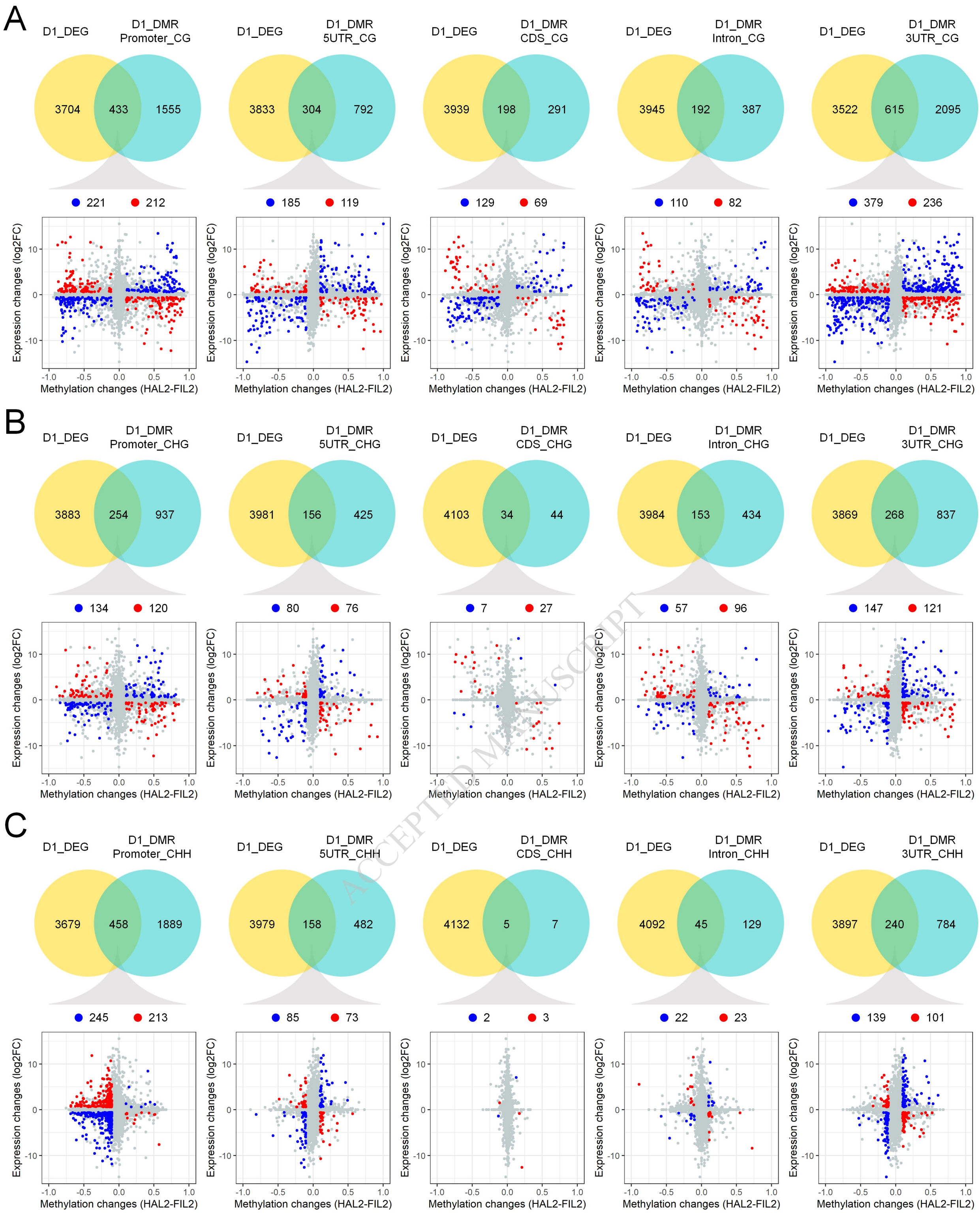

Figure 7. Association of differentially methylated genes with differentially expressed genes.
Venn diagrams depicting the number of differentially expressed genes (yellow circle, DEGs) and differentially methylated regions (DMRs)-associated genes (blue circle, DMR) between HAL2 and FIL2 D1 inflorescence in CG (A), CHG (B), and CHH (C) contexts across five different genomic features. Two-dimensional scatter plots depict the association of differentially expressed genes and differentially methylated regions in CG (A), CHG (B), and CHH (C) contexts across five different genomic features. The *x*-axis represents relative gene expression change (log2fold change), while the *y*-axis represents relative methylation change (HAL2 subtracted from FIL2). The data for the association of differentially methylated genes with differentially expressed genes at D4 inflorescence are given in Supplemental Figure S18.

Figure 8. Evolution of differentially methylated regions-associated differentially expressed gene pairs.

(A) and (B) The K_a/K_s values distribution of gene pairs from differentially methylated regions (DMRs)-associated differentially expressed genes (DEGs) and one-to-one putative orthologs between HAL2 and FIL2. (A) The mean values are indicated by the dashed line. (B) The solid black line marks $K_a/K_s = 1$. The red dots mark the DMRs-associated DEGs with K_a/K_s ratio larger than 1, while the blue dots mark the DMRs-associated DEGs with K_a/K_s ratio less than 1. The grey dots represent all one-to-one putative orthologs. (C) Differential methylation patterns of CG, CHG, and CHH contexts across five different genomic features for DMRs-associated DEGs genes that are putatively positively selected. In all panels, the bar plots and error bars are the average values and *SE*, respectively, based on methylation level from three replicates. (D) Expression patterns of DMRs-associated DEGs genes that are putatively positively selected. The *x*-axis represents four developmental stages, while the *y*-axis represents normalized counts using variance stabilizing transformation in DEseq2. In all panels, the points and error bars are the average values and *SE*, respectively, based on normalized counts of three RNA-seq replicates.

Parsed Citations

Ashikari M, Sakakibara H, Lin SY, Yamamoto T, Takashi T, Nishimura A, Angeles ER, Qian Q, Kitano H, Matsuoka M (2005) Cytokinin oxidase regulates rice grain production. Science 309: 741-745
Google Scholar: Author Only Title Only Author and Title

Barazesh S, McSteen P (2008) Hormonal control of grass inflorescence development. Trends Plant Sci 13: 656-662
Google Scholar: Author Only Title Only Author and Title

Bartrina I, Otto E, Strnad M, Werner T, Schmulling T (2011) Cytokinin regulates the activity of reproductive meristems, flower organ size, ovule formation, and thus seed yield in Arabidopsis thaliana. Plant Cell 23: 69-80
Google Scholar: Author Only Title Only Author and Title

Bess EC, Doust AN, Kellogg EA (2005) A naked grass in the "bristle clade": a phylogenetic and developmental study of Panicum section Bulbosa (Paniceae : Poaceae). Int J Plant Sci 166: 371-381
Google Scholar: Author Only Title Only Author and Title

Bewick AJ, Schmitz RJ (2017) Gene body DNA methylation in plants. Curr Opin Plant Biol 36: 103-110
Google Scholar: Author Only Title Only Author and Title

Bolduc N, Hake S (2009) The maize transcription factor KNOTTED1 directly regulates the gibberellin catabolism gene ga2ox1. Plant Cell 21: 1647- 1658
Google Scholar: Author Only Title Only Author and Title

Bouche N, Lauressergues D, Gasciolli V, Vaucheret H (2006) An antagonistic function for Arabidopsis DCL2 in development and a new function for DCL4 in generating viral siRNAs. EMBO J 25: 3347-3356
Google Scholar: Author Only Title Only Author and Title

Buendia-Monreal M, Gillmor CS (2018) The times they are a-changin': heterochrony in plant development and evolution. Front Plant Sci 9: 1349
Google Scholar: Author Only Title Only Author and Title

Chan SW, Henderson IR, Jacobsen SE (2005) Gardening the genome: DNA methylation in Arabidopsis thaliana. Nat Rev Genet 6: 351-360
Google Scholar: Author Only Title Only Author and Title

Chen CJ, Chen H, Zhang Y, Thomas HR, Frank MH, He YH, Xia R (2020) TBtools: an integrative toolkit developed for interactive analyses of big biological data. Mol Plant 13: 1194-1202
Google Scholar: Author Only Title Only Author and Title

Conway JR, Lex A, Gehlenborg N (2017) UpSetR: an R package for the visualization of intersecting sets and their properties. Bioinformatics 33: 2938-2940
Google Scholar: Author Only Title Only Author and Title

Dai XH, Liu ZH, Qiao M, Li J, Li S, Xiang FN (2017) ARR12 promotes de novo shoot regeneration in Arabidopsis thaliana via activation of WUSCHEL expression. J Integr Plant Biol 59: 747-758
Google Scholar: Author Only Title Only Author and Title

Deveshwar P, Prusty A, Sharma S, Tyagi AK (2020) Phytohormone-mediated molecular mechanisms involving multiple genes and QTL govern grain number in rice. Front Genet 11: 586462
Google Scholar: Author Only Title Only Author and Title

Eveland AL, Goldshmidt A, Pautler M, Morohashi K, Liseron-Monfils C, Lewis MW, Kumari S, Hiraga S, Yang F, Unger-Wallace E, Olson A, Hake S, Vollbrecht E, Grotewold E, Ware D, Jackson D (2014) Regulatory modules controlling maize inflorescence architecture. Genome Res 24: 431-443
Google Scholar: Author Only Title Only Author and Title

Feng N, Song GY, Guan JT, Chen K, Jia ML, Huang DH, Wu JJ, Zhang LC, Kong XY, Geng SF, Liu J, Li AL, Mao L (2017) Transcriptome profiling of wheat inflorescence development from spikelet initiation to floral patterning identified stage-specific regulatory genes. Plant Physiol 174: 1779-1794
Google Scholar: Author Only Title Only Author and Title

Fernandez-Nohales P, Domenech MJ, Martinez de Alba AE, Micol JL, Ponce MR, Madueno F (2014) AGO1 controls arabidopsis inflorescence architecture possibly by regulating TFL1 expression. Ann Bot 114: 1471-1481
Google Scholar: Author Only Title Only Author and Title

Furutani I, Sukegawa S, Kyozuka J (2006) Genome-wide analysis of spatial and temporal gene expression in rice panicle development. Plant J 46: 503-511
Google Scholar: Author Only Title Only Author and Title

Gould BA, Palacio-Mejia JD, Jenkins J, Mamidi S, Barry K, Schmutz J, Juenger TE, Lowry DB (2018) Population genomics and climate adaptation of a C4 perennial grass, Panicum hallii (Poaceae). BMC Genomics 19: 792
Google Scholar: Author Only Title Only Author and Title

Gu ZG, Eils R, Schlesner M (2016) Complex heatmaps reveal patterns and correlations in multidimensional genomic data. Bioinformatics 32: 2847-2849
Google Scholar: Author Only Title Only Author and Title

Harder LD, Prusinkiewicz P (2013) The interplay between inflorescence development and function as the crucible of architectural diversity. Ann Bot 112: 1477-1493
Google Scholar: Author Only Title Only Author and Title

Harrop TW, Ud Din I, Gregis V, Osnato M, Jouannic S, Adam H, Kater MM (2016) Gene expression profiling of reproductive meristem types in early rice inflorescences by laser microdissection. Plant J 86: 75-88
Google Scholar: Author Only Title Only Author and Title

Higo A, Saihara N, Miura F, Higashi Y, Yamada M, Tamaki S, Ito T, Tarutani Y, Sakamoto T, Fujiwara M, Kurata T, Fukao Y, Moritoh S, Terada R, Kinoshita T, Ito T, Kakutani T, Shimamoto K, Tsuji H (2020) DNA methylation is reconfigured at the onset of reproduction in rice shoot apical meristem. Nat Commun 11: 4079
Google Scholar: Author Only Title Only Author and Title

Huang H, Liu RE, Niu QF, Tang K, Zhang B, Zhang H, Chen KS, Zhu JK, Lang ZB (2019) Global increase in DNA methylation during orange fruit development and ripening. Proc Natl Acad Sci USA 116: 1430-1436
Google Scholar: Author Only Title Only Author and Title

Huang XS, Zhang SL, Li KQ, Thimmapuram J, Xie SJ, Wren J (2018) ViewBS: a powerful toolkit for visualization of high-throughput bisulfite sequencing data. Bioinformatics 34: 708-709
Google Scholar: Author Only Title Only Author and Title

Jia SZ, Xiong YF, Xiao PP, Wang X, Yao JL (2019) OsNF-YC10, a seed preferentially expressed gene regulates grain width by affecting cell proliferation in rice. Plant Sci 280: 219-227
Google Scholar: Author Only Title Only Author and Title

Kawakatsu T, Huang SC, Jupe F, Sasaki E, Schmitz RJ, Urich MA, Castanon R, Nery JR, Barragan C, He Y, Chen H, Dubin M, Lee CR, Wang C, Bemm F, Becker C, O'Neil R, O'Malley RC, Quarless DX, Genomes C, Schork NJ, Weigel D, Nordborg M, Ecker JR (2016) Epigenomic diversity in a global collection of Arabidopsis thaliana accessions. Cell 166: 492-505
Google Scholar: Author Only Title Only Author and Title

Kellogg EA, Camara PEAS, Rudall PJ, Ladd P, Malcomber ST, Whipple CJ, Doust AN (2013) Early inflorescence development in the grasses (Poaceae). Front Plant Sci 4: 250
Google Scholar: Author Only Title Only Author and Title

Kellogg EA (2022) Genetic control of branching patterns in grass inflorescences. Plant Cell 34: 2518-2533
Google Scholar: Author Only Title Only Author and Title

Khasanova A, Lovell JT, Bonnette J, Weng XY, Jenkins J, Yoshinaga Y, Schmutz J, Juenger TE (2019) The genetic architecture of shoot and root trait divergence between mesic and xeric ecotypes of a perennial grass. Front Plant Sci 10: 366
Google Scholar: Author Only Title Only Author and Title

Koo BH, Yoo SC, Park JW, Kwon CT, Lee BD, An G, Zhang ZY, Li JJ, Li ZC, Paek NC (2013) Natural variation in OsPRR37 regulates heading date and contributes to rice cultivation at a wide range of latitudes. Mol Plant 6: 1877-1888
Google Scholar: Author Only Title Only Author and Title

Krueger F, Andrews SR (2011) Bismark: a flexible aligner and methylation caller for Bisulfite-Seq applications. Bioinformatics 27: 1571-1572
Google Scholar: Author Only Title Only Author and Title

Kumar L, M EF (2007) Mfuzz: a software package for soft clustering of microarray data. Bioinformation 2: 5-7
Google Scholar: Author Only Title Only Author and Title

Kurakawa T, Ueda N, Maekawa M, Kobayashi K, Kojima M, Nagato Y, Sakakibara H, Kyozuka J (2007) Direct control of shoot meristem activity by a cytokinin-activating enzyme. Nature 445: 652-655
Google Scholar: Author Only Title Only Author and Title

Kyozuka J, Tokunaga H, Yoshida A (2014) Control of grass inflorescence form by the fine-tuning of meristem phase change. Curr Opin Plant Biol 17: 110-115
Google Scholar: Author Only Title Only Author and Title

Law JA, Jacobsen SE (2010) Establishing, maintaining and modifying DNA methylation patterns in plants and animals. Nat Rev Genet 11: 204-220

Google Scholar: Author Only Title Only Author and Title

Lee DY, Lee J, Moon S, Park SY, An G (2007) The rice heterochronic gene SUPERNUMERARY BRACT regulates the transition from spikelet meristem to floral meristem. Plant J 49: 64-78
Google Scholar: Author Only Title Only Author and Title

Li X, Zhu JD, Hu FY, Ge S, Ye MZ, Xiang H, Zhang GJ, Zheng XM, Zhang HY, Zhang SL, Li Q, Luo RB, Yu C, Yu J, Sun JF, Zou XY, Cao XF, Xie XF, Wang J, Wang W (2012) Single-base resolution maps of cultivated and wild rice methylomes and regulatory roles of DNA methylation in plant gene expression. BMC Genomics 13: 300
Google Scholar: Author Only Title Only Author and Title

Li ZQ, Tang MQ, Luo DJ, Kashif MH, Cao S, Zhang WX, Hu YL, Huang Z, Yue J, Li R, Chen P (2021) Integrated methylome and transcriptome analyses reveal the molecular mechanism by which DNA methylation regulates Kenaf flowering. Front Plant Sci 12: 709030
Google Scholar: Author Only Title Only Author and Title

Liao PF, Ouyang JX, Zhang JJ, Yang L, Wang X, Peng XJ, Wang D, Zhu YL, Li SB (2019) OsDCL3b affects grain yield and quality in rice. Plant Mol Biol 99: 193-204
Google Scholar: Author Only Title Only Author and Title

Liu C, Teo ZW, Bi Y, Song SY, Xi WY, Yang XB, Yin ZC, Yu H (2013) A conserved genetic pathway determines inflorescence architecture in Arabidopsis and rice. Dev Cell 24: 612-622
Google Scholar: Author Only Title Only Author and Title

Love MI, Huber W, Anders S (2014) Moderated estimation of fold change and dispersion for RNA-seq data with DESeq2. Genome Biol 15: 550
Google Scholar: Author Only Title Only Author and Title

Lovell JT, Jenkins J, Lowry DB, Mamidi S, Sreedasyam A, Weng XY, Barry K, Bonnette J, Campitelli B, Daum C, Gordon SP, Gould BA, Khasanova A, Lipzen A, MacQueen A, Palacio-Mejia JD, Plott C, Shakirov EV, Shu SQ, Yoshinaga Y, Zane M, Kudrna D, Talag JD, Rokhsar D, Grimwood J, Schmutz J, Juenger TE (2018) The genomic landscape of molecular responses to natural drought stress in Panicum hallii. Nat Commun 9: 5213
Google Scholar: Author Only Title Only Author and Title

Lovell JT, Schwartz S, Lowry DB, Shakirov EV, Bonnette JE, Weng XY, Wang M, Johnson J, Sreedasyam A, Plott C, Jenkins J, Schmutz J, Juenger TE (2016) Drought responsive gene expression regulatory divergence between upland and lowland ecotypes of a perennial C4 grass. Genome Res 26: 510-518
Google Scholar: Author Only Title Only Author and Title

Lowry DB, Hernandez K, Taylor SH, Meyer E, Logan TL, Barry KW, Chapman JA, Rokhsar DS, Schmutz J, Juenger TE (2015) The genetics of divergence and reproductive isolation between ecotypes of Panicum hallii. New Phytol 205: 402-414
Google Scholar: Author Only Title Only Author and Title

Martin GT, Seymour DK, Gaut BS (2021) CHH methylation islands: a nonconserved feature of grass genomes that is positively associated with transposable elements but negatively associated with gene-body methylation. Genome Biol Evol 13: evab144
Google Scholar: Author Only Title Only Author and Title

Moritoh S, Eun CH, Ono A, Asao H, Okano Y, Yamaguchi K, Shimatani Z, Koizumi A, Terada R (2012) Targeted disruption of an orthologue of DOMAINS REARRANGED METHYLASE 2, OsDRM2, impairs the growth of rice plants by abnormal DNA methylation. Plant J 71: 85-98
Google Scholar: Author Only Title Only Author and Title

Niederhuth CE, Bewick AJ, Ji L, Alabady MS, Kim KD, Li Q, Rohr NA, Rambani A, Burke JM, Udall JA, Egesi C, Schmutz J, Grimwood J, Jackson SA, Springer NM, Schmitz RJ (2016) Widespread natural variation of DNA methylation within angiosperms. Genome Biol 17: 194
Google Scholar: Author Only Title Only Author and Title

Palacio-Mejia JD, Grabowski PP, Ortiz EM, Silva-Arias GA, Haque T, Des Marais DL, Bonnette J, Lowry DB, Juenger TE (2021) Geographic patterns of genomic diversity and structure in the C4 grass Panicum hallii across its natural distribution. AoB Plants 13: plab002
Google Scholar: Author Only Title Only Author and Title

Parvathaneni RK, Bertolini E, Shamimuzzaman M, Vera DL, Lung PY, Rice BR, Zhang JF, Brown PJ, Lipka AE, Bass HW, Eveland AL (2020) The regulatory landscape of early maize inflorescence development. Genome Biol 21: 165
Google Scholar: Author Only Title Only Author and Title

Rajkumar MS, Gupta K, Khemka NK, Garg R, Jain M (2020) DNA methylation reprogramming during seed development and its functional relevance in seed size/weight determination in chickpea. Commun Biol 3: 340
Google Scholar: Author Only Title Only Author and Title

Rao NN, Prasad K, Kumar PR, Vijayraghavan U (2008) Distinct regulatory role for RFL, the rice LFY homolog, in determining flowering time and plant architecture. Proc Natl Acad Sci U S A 105: 3646-3651
Google Scholar: Author Only Title Only Author and Title

Razzaque S, Juenger TE (2022) The ecology and quantitative genetics of seed and seedling traits in upland and lowland ecotypes of a perennial grass. Evol Lett 6: 460-473
Google Scholar: Author Only Title Only Author and Title

Sadras VO (2007) Evolutionary aspects of the trade-off between seed size and number in crops. Field Crops Res 100: 125-138
Google Scholar: Author Only Title Only Author and Title

Shi Y, Zhang XT, Chang XJ, Yan MK, Zhao HM, Qin Y, Wang HF (2021) Integrated analysis of DNA methylome and transcriptome reveals epigenetic regulation of CAM photosynthesis in pineapple. BMC Plant Biol 21: 19
Google Scholar: Author Only Title Only Author and Title

Sreedasyam A, Plott C, Hossain MS, Lovell JT, Grimwood J, Jenkins JW, Daum C, Barry K, Carlson J, Shu SQ, Phillips J, Amirebrahimi M, Zane M, Wang M, Goodstein D, Haas FB, Hiss M, Perroud P-F, Jawdy SS, Hu R, Johnson J, Kropat J, Gallaher SD, Lipzen A, Tillman R, Shakirov EV, Weng XY, Torres-Jerez I, Weers B, Conde D, Pappas MR, Liu LF, Muchlinski A, Jiang H, Shyu C, Huang P, Sebastian J, Laiben C, Medlin A, Carey S, Carrell AA, Perales M, Swaminathan K, Allona I, Grattapaglia D, Cooper EA, Tholl D, Vogel JP, Weston DJ, Yang XH, Brutnell TP, Kellogg EA, Baxter I, Udvardi M, Tang YH, Mockler TC, Juenger TE, Mullet J, Rensing SA, Tuskan GA, Merchant SS, Stacey G, Schmutz J (2022) JGI Plant Gene Atlas: An updateable transcriptome resource to improve structural annotations and functional gene descriptions across the plant kingdom. BioRxiv: 2022.09.30.510380
Google Scholar: Author Only Title Only Author and Title

Sun YH, Dong L, Zhang Y, Lin D, Xu WZ, Ke CX, Han LQ, Deng LL, Li GL, Jackson D, Li XW, Yang F (2020) 3D genome architecture coordinates trans and cis regulation of differentially expressed ear and tassel genes in maize. Genome Biol 21: 143
Google Scholar: Author Only Title Only Author and Title

Tate PH, Bird AP (1993) Effects of DNA methylation on DNA-binding proteins and gene expression. Curr Opin Genet Dev 3: 226-231
Google Scholar: Author Only Title Only Author and Title

Teo ZWN, Song SY, Wang YQ, Liu J, Yu H (2014) New insights into the regulation of inflorescence architecture. Trends in Plant Sci 19: 158-165
Google Scholar: Author Only Title Only Author and Title

Tu CW, Li TT, Liu XY (2019) Genetic and epigenetic regulatory mechanism of rice panicle development. 2018 International Conference on Biotechnology and Bioengineering (8th Icbb) 2079: 020001
Google Scholar: Author Only Title Only Author and Title

Wang L, Sun SY, Jin JY, Fu DB, Yang XF, Weng XY, Xu CG, Li XH, Xiao JH, Zhang QF (2015) Coordinated regulation of vegetative and reproductive branching in rice. Proc Natl Acad Sci USA 112: 15504-15509
Google Scholar: Author Only Title Only Author and Title

Wang L, Xie WB, Chen Y, Tang WJ, Yang JY, Ye RJ, Liu L, Lin YJ, Xu CG, Xiao JH, Zhang QF (2010) A dynamic gene expression atlas covering the entire life cycle of rice. Plant J 61: 752-766
Google Scholar: Author Only Title Only Author and Title

Weng XY, Lovell JT, Schwartz SL, Cheng CD, Haque T, Zhang L, Razzaque S, Juenger TE (2019) Complex interactions between day length and diurnal patterns of gene expression drive photoperiodic responses in a perennial C4 grass. Plant Cell Environ 42: 2165-2182
Google Scholar: Author Only Title Only Author and Title

Wulfridge P, Langmead B, Feinberg AP, Hansen KD (2019) Analyzing whole genome bisulfite sequencing data from highly divergent genotypes. Nucleic Acids Res 47: e117
Google Scholar: Author Only Title Only Author and Title

Xu G, Lyu J, Li Q, Liu H, Wang DF, Zhang M, Springer NM, Ross-Ibarra J, Yang JL (2020) Evolutionary and functional genomics of DNA methylation in maize domestication and improvement. Nat Commun 11: 5539
Google Scholar: Author Only Title Only Author and Title

Yan WH, Liu HY, Zhou XC, Li QP, Zhang J, Lu L, Liu TM, Liu HJ, Zhang CJ, Zhang ZY, Shen GJ, Yao W, Chen HX, Yu SB, Xie WB, Xing YZ (2013) Natural variation in Ghd7.1 plays an important role in grain yield and adaptation in rice. Cell Res 23: 969-971
Google Scholar: Author Only Title Only Author and Title

Yang HX, Chang F, You CJ, Cui J, Zhu GF, Wang L, Zheng Y, Qi J, Ma H (2015) Whole-genome DNA methylation patterns and complex associations with gene structure and expression during flower development in Arabidopsis. Plant J 81: 268-281
Google Scholar: Author Only Title Only Author and Title

Zhang DB, Yuan Z (2014) Molecular control of grass inflorescence development. Annu Rev Plant Biol 65: 553-578
Google Scholar: Author Only Title Only Author and Title

Zhang H, Zhu SS, Liu TZ, Wang CM, Cheng ZJ, Zhang X, Chen LP, Sheng PK, Cai MH, Li CN, Wang JC, Zhang Z, Chai JT, Zhou L, Lei CL, Guo XP, Wang JL, Wang J, Jiang L, Wu CY, Wan JM (2019) DELAYED HEADING DATE1 interacts with OsHAP5C/D, delays flowering time and enhances yield in rice. Plant Biotechnol J 17: 531-539
Google Scholar: Author Only Title Only Author and Title

Zhang HM, Lang ZB, Zhu JK (2018) Dynamics and function of DNA methylation in plants. Nat Rev Mol Cell Biol 19: 489-506
Google Scholar: Author Only Title Only Author and Title

Zhang L, Yu H, Ma B, Liu GF, Wang JJ, Wang JM, Gao RC, Li JJ, Liu JY, Xu J, Zhang YY, Li Q, Huang XH, Xu JL, Li JM, Qian Q, Han B, He ZH, Li JY (2017) A natural tandem array alleviates epigenetic repression of IPA1 and leads to superior yielding rice. Nat Commun 8: 14789
Google Scholar: Author Only Title Only Author and Title

Zhu CM, Yang J, Box MS, Kellogg EA, Eveland AL (2018) A dynamic co-expression map of early inflorescence development in Setaria viridis provides a resource for gene discovery and comparative genomics. Front Plant Sci 9: 1309
Google Scholar: Author Only Title Only Author and Title

Zhu ZF, Tan LB, Fu YC, Liu FX, Cai HW, Xie DX, Wu F, Wu JZ, Matsumoto T, Sun CQ (2013) Genetic control of inflorescence architecture during rice domestication. Nat Commun 4: 2200
Google Scholar: Author Only Title Only Author and Title